POLITECNICO DI TORINO

Master's Degree in Biomedical Engineering

Politecnico
di Torino

OPTIMIZATION OF TUMOR LASER ABLATION

Evaluation of thermal properties: the liver tissue case

Supervisors

Prof. Guido PERRONE

Prof. Gianni COPPA

Prof. Alberto VALLAN

Candidate

Francesca LUCHETTA

Academic Year 2020/2021

Summary

Cancer represents one of the main causes of death worldwide, moreover with an increasing occurrence trend. In particular, liver cancer represents the sixth most common tumor, with still a pretty low relative survival rate despite the research advancements in the last decades. The elective treatment for liver tumors is surgery and a lot of effort has been devoted in finding new intervention techniques that can combine high efficacy with lower patient discomfort. Among them, minimally invasive methods that induce a controlled tissue hyperthermia (radiofrequency, microwave, and laser ablations) have risen great interest because they represent a valid alternative to standard surgical resection, which is not always possible due to the peculiar characteristics of the malignant lesion or the patient general health conditions. This thesis focuses on Laser Ablation (LA), a treatment in which the cytotoxic temperature is reached exploiting the absorption of laser light delivered to the tumor site by an optical fibre applicator. Despite the many advantages of LA (for instance, the localized heating that minimizes the effects on healthy tissue and the possibility to carry out the ablation under imaging methods like the magnetic resonance), this technique is not as widely employed as other forms of ablation. This mainly because of the lack of an accurate treatment planning tool, in turn due to the difficulty to predict the outcomes given the large variability of the optical (absorption) and thermal (conductivity) parameters of the liver tissue with the location of the malignancy. The aim of this thesis project is to investigate the thermal properties of liver in view of the integration of a more realistic thermal model in a laser ablation planning tool to be used for the real-time monitoring of the LA procedure. The fundamental idea is to retrieve information on the thermal properties – mainly the thermal diffusivity – in real time by generating a small tissue heating with the laser before the proper laser ablation procedure. To this end, two methods to estimate the thermal parameters starting from the experimental temperature curves have been studied and a thermal model has been developed, solving the heat equation using the Partial Differential Equation (PDE) toolbox of MATLAB®. The procedure was experimentally validated using for simplicity ex-vivo bovine liver tissue. Clearly, using ex-vivo tissue does not allow considering all the biological phenomena, such as the impact of perfusion in the

body thermoregulation; however, despite this limit, it provides a good starting point for understanding the variability of the thermal diffusivity. Extensive tests at different laser powers and irradiation times were performed in different ex-vivo bovine tissues. To avoid artifacts due to the interaction between the laser beam and the sensor, the temperature variations were recorded using all dielectric sensor arrays based on Fibre Bragg Gratings (FBGs).

Table of Contents

List of Tables

List of Figures

Acronyms

CW
Continuous Wave

FBG
Fibre Bragg Grating

FOS
Fibre Optic Sensor

HCC
HepatoCellular Carcinoma

HIFU
High-Intensity Focused Ultrasound

FEM
Finite Element Method

LA
Laser Ablation

LASER
Light Amplification by Stimulated Emission of Radiation

MWA
MicroWave Ablation

PDE
Partial Differential Equation

PW

Pulsed Wave

RFA

RadioFrequency Ablation

Chapter 1

Introduction

One of the main challenges that the scientific community is carrying on is fighting cancers, as they are among the leading causes of death worldwide. Tumors consist in an uncontrolled proliferation of cells that are different in shape and function to the healthy ones. The proliferation is due to an alteration in the genetic heritage of some cells, which causes the disruption of the healthy homeostasis between the phenomena of normal cell division and apoptosis (programmed cells death). In terms of incidence the six leading cancer types are breast, lung, colorectum, prostate, stomach, liver and cervix uteri tumors, representing more than 50% of new diagnosed cancer cases in 2020. Liver cancer, in particular, with 905.677 new cases in 2020, is the sixth most frequent type of cancer (Fig. 1.1)[1, 2].

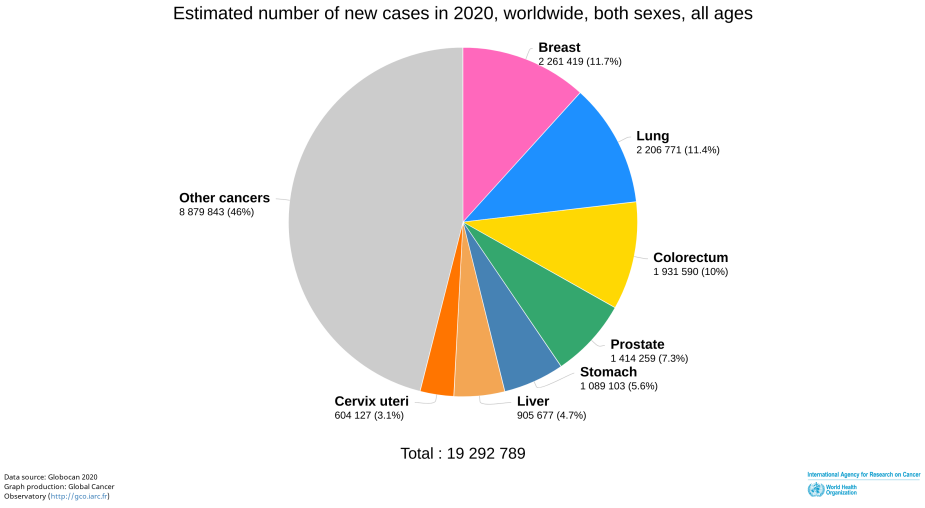

Figure 1.1: Estimated worldwide number of new cancer cases in 2020, for both sexes and all ages [1].

Liver tumors, like other cancers, can be classified as *primary* or *secondary*, depending on the origin of cancer. Primary tumors originate from the liver structures, like the *hepatocellular carcinoma*, which is the most common primary tumor forming from liver cells. Secondary tumors, also called *metastasis*, form when cancer cells move from the site where they originated to another area. Since the liver acts as a filter for the organism, it receives blood from many parts of the body. It means that the liver is one of the most common locations for metastasis. For this reason, secondary liver tumors are more common than primary [2].

The incidence of liver tumor in the United States showed, in the last years, a constant trend in men and a growth rate of 2% per year for women. Despite this, the incidence in men is higher than women (Fig. 1.2) [3].

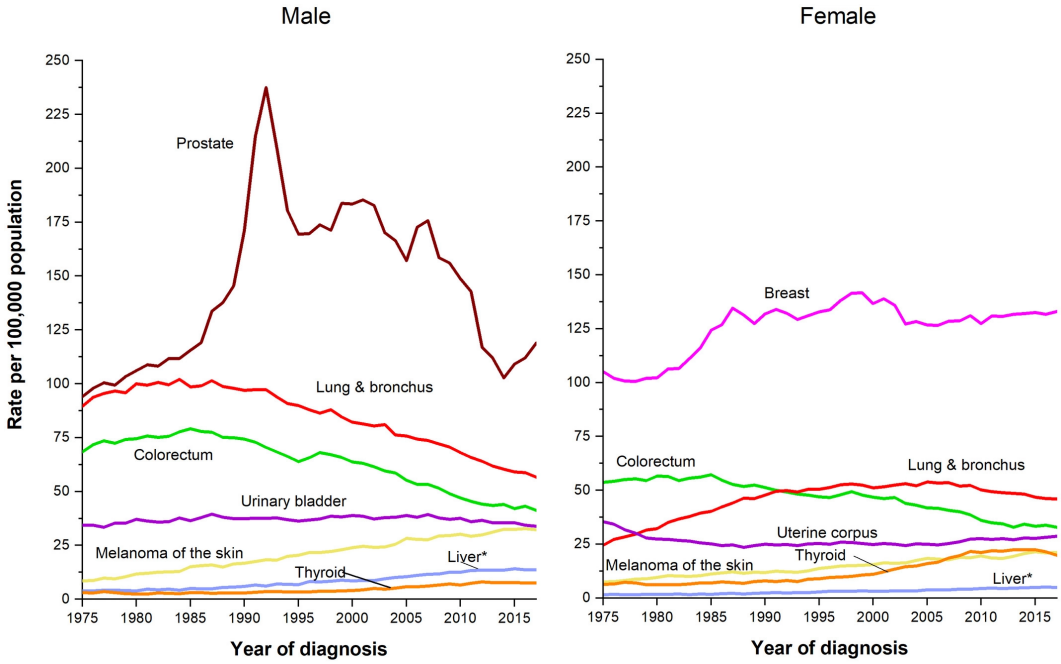

Figure 1.2: Trends in incidence rates for selected cancers by sex, United States, 1975 to 2017 [3].

The predominance of the male sex is also found in the 2020 data relating to deaths from cancer. Liver cancer, in fact, represented the second cause of death from cancer in men and the sixth for women, remaining however the third type of cancer for number of deaths considering both sexes (Fig. 1.3) [1].

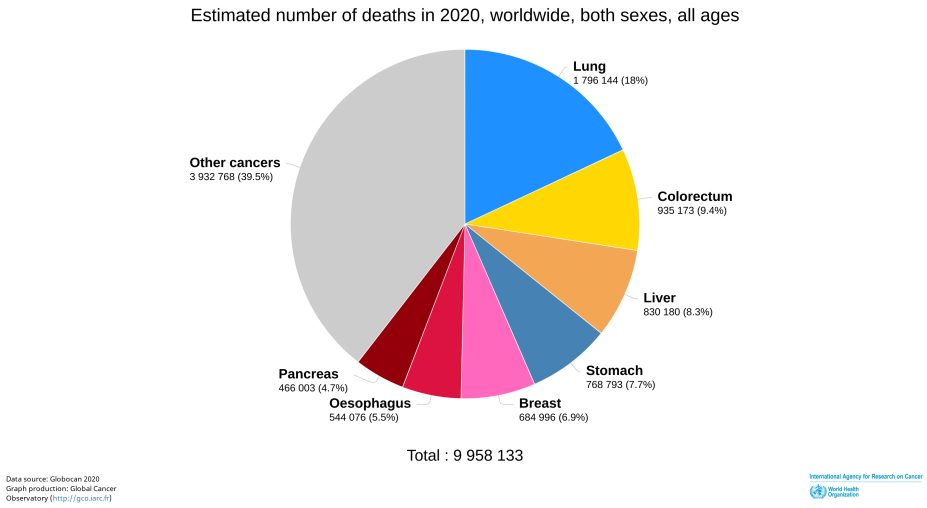

Figure 1.3: Estimated worldwide number of deaths in 2020 considering both sexes and all ages [1].

According to the forecast, the estimated numbers of new cases and deaths in the world from 2020 to 2040 for liver cancer are both growing (Fig. 1.4) [1].

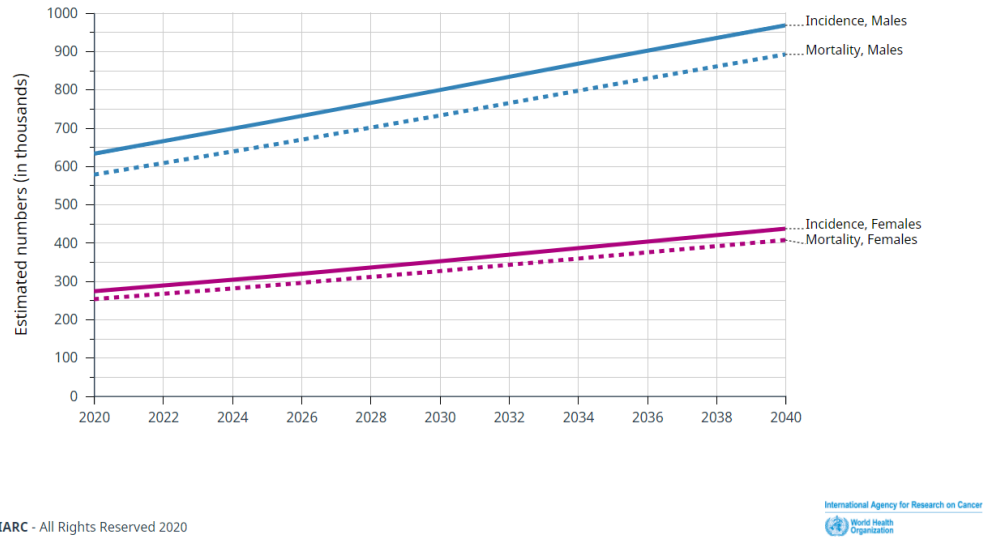

Figure 1.4: Estimated incidence and death trends from 2020 to 2040 for bot sexes and all ages [1].

Nowadays the elective treatment for liver tumors is surgery resection. Unfortunately, surgery is not always a viable option, depending on the characteristics of

the malignant lesion and the patient general health conditions. Extension, position and number of lesions and the residual functionality of the liver are significant aspects to be considered for this purpose [2]. Among the alternative to the standard surgery, minimally invasive treatments are widely spreading as they combine high efficacy with lower patient discomfort. These treatments induce a controlled tissue hyperthermia or hypothermia in order to cause the death of tumor cells, avoiding damaging the healthy tissues surrounding the lesion.

This thesis project focuses on Laser Ablation (LA) technique, an innovative strategy in which the cytotoxic temperature is reached exploiting the absorption of laser light delivered to the tumor site by optical fibres. Laser ablation has raised a great interest in the medical field. Among the great advantages, the possibility to have a localized heating that minimizes the effects on healthy tissue, the electromagnetic compatibility that permits to carry out the ablation under imaging methods like the magnetic resonance, and the possibility to expand the intervention area by using several (usually, up to four) light delivery applicators. Despite the advantages, LA treatments are currently not widely used procedures, since the other ablation techniques are more consolidated (e.g., radio-frequency ablation and microwave ablation); moreover, the control of some ablation aspects is still difficult. For instance, the accurate prediction of the affected area during a laser ablation process is a major challenge because it depends on numerous factors including the thermal and optical properties of the ablated tissue, characterized by a great variability. This results in the lack of an accurate treatment planning tool.

The aim of this thesis is to study the thermal properties of the liver tissue in order to optimize the laser ablation treatment.

For this purpose, some experimental tests on ex-vivo bovine liver tissue have been conducted. Unfortunately, working on ex-vivo bovine tissue does not allow considering all the possible biological phenomena that would influence in vivo ablations, such as the heat-sink effect due to perfusion, which would cause energy losses. However, the results obtained from these tests can represent a starting point for evaluations in more realistic cases and for understanding the variability of the thermal properties. A laser light delivered to the tissue by an optical fibre applicator has been used to induce a small tissue heating. The temperature variations in some points of the tissue have been measured by sensor arrays based on Fibre Bragg Gratings (FBGs). Two possible methods have been developed to obtain information about thermal properties - mostly the thermal diffusivity - from the experimental temperature curves recorded. A thermal model has been created in MATLAB® to validate them. The heat equation has been solved by using the Partial Differential Equation (PDE) toolbox of MATLAB®.

Chapter 2

Energy-based procedures for tumor ablation

This section provides a brief introduction to the most common minimally invasive techniques for treating solid tumors as alternatives to standard surgical resection, which is not always feasible. The main focus is on treatments based on thermal energy.

2.1 Tumor ablation

In the context of tumors, ablation means the application of some factors to the malignant cells to induce their death, while protecting healthy cells from exposure.

Tumor ablation treatments are divided into chemically-based and energy-based procedures depending on whether the tumor is removed by direct application of chemicals or energy (Fig. 2.1). The term "direct" is used to indicate that these techniques involve therapies applied at the tumor site rather than orally or via an intravascular route [4].

Thermal energy-based treatments consist in a localised application of extreme temperatures in order to induce irreversible damages to the cancer cells and coagulative necrosis. The temperatures reached in the lesion site can be both high and low.
During heating thermoablative procedures electromagnetic radiations at different frequencies are used to achieve and maintain a temperature from 50 °C to 100 °C into the entire target tumor volume. The energy source is delivered to the tumor site using applicators inserted through the skin, resulting in a minimally-invasive treatment that limit the recovery time for the patient and the risk of possible

complications after surgery compared to what happens after surgical resection. The insertion of applicators is performed under image guided procedures such as with Magnetic Resonance (MR), Ultrasounds (US),or Computed Tomography (CT).

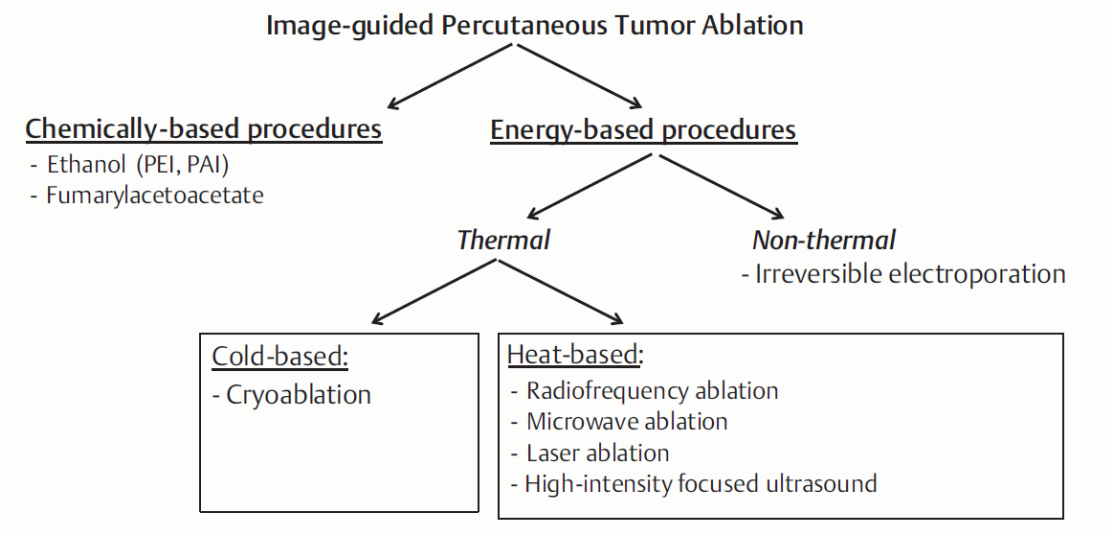

Figure 2.1: Classification of tumor ablation procedures [5].

Among the heating thermoablative procedures there are:

- ***RadioFrequency Ablation (RFA)*** [4, 6]
  It is the most used, optimized and effective ablative technique. It is the first viable alternative for HepatoCellular Carcinoma (HCC) removal in patients not eligible for surgical resection, being as effective as the latter in the treatment of small and centrally located HCC. The technique involves the achievement of a high temperature in the tumor by injection of an alternating current (350-500 kHz) through an electrode. Injection of a radiofrequency current avoids the risk of electrical stimulation of the heart and nerves. This current, while propagating, causes ionic agitation in the tissues and a frictional heating. The coagulative necrosis of the tumor is induced by reaching a temperature of minimum 60 °C. Devices for RFA are divided into *monopolar* and *bipolar* systems. In monopolar systems, the most used, the injection current electrode is inserted into the tumor and a neutral electrode is placed on the body surface. In bipolar systems two "active" electrodes are placed close together inside the malignant lesion. Among the limits of RFA, the dependence of efficacy on tumor location and size and the inhability of treating tumors close to large vessels, due to the heat-sink effect which does not permit reaching local overheating;

- ***MicroWave Ablation (MWA)*** [6].
  It involves the insertion of an interstitial antenna emitting high-frequency electromagnetic radiations (900 MHz to 2,500 MHz), which cause the oscillation of polar molecules in tissue. This results in an increase in the kinetic energy of the molecules and in an overheating of the tissue that causes coagulative necrosis. Unlike RFA, MWA does not require a conductive path to induce temperature variation. It means that microwaves can propagate also in tissues with low electrical conductivity, low thermal conductivity and high impedance. Moreover, the application of grounding pads is not necessary. Among the major advantages of MWA, the possibility of producing faster heating in larger tissue volumes with limited sensitivity to physiological heat dissipation effects, the deeper penetration of radiations and the possibility of inducing higher local temperatures. Despite the many theoretical advantages, this treatment still presents many difficulties of application. The high material costs, the overheating of the cables necessary for the transport of microwaves and the excessive flexibility of the antennas are the main limitations of the treatment;

- ***High-Intensity Focused Ultrasound (HIFU)***
  It is a technique in which localized necrosis is induced by the application of high intensity ultrasound produced by a piezoelectric transducer and focused on the tumor volume through lens. In this case, the thermal energy is obtained as a result of a mechanical energy of sound waves conversion into tissues. The ultrasonic beam can be focused to a single point if the tumor mass is small or concentrated in several points;

- ***Laser Ablation (LA)*** [5, 6, 7]
  It is one of the most recent strategies for treating tumors through thermal energy application. In LA, necrosis is caused by the absorption of light energy, which is directly applied inside the tumour via flexible thin optical fibres (200 µm to 600 µm) inserted through needles. The possibility of using all-dielectric applicators makes LA the only technique fully compatible with Magnetic Resonance Imaging (MRI). The most common laser sources are those based on Neodymiun-doped Yttrium Aluminum Garnet (Nd-YAG) lasers, with emission wavelength of 1,064 nm, and on diode lasers, with emission wavelength from 800 nm to 980 nm. These wavelengths, which are in the Near Infra-Red (NIR), represents the best compromise between absorption and penetration capabilities. Beam-splitting devices or multi-source devices can be used to deliver the light through different fibres and thus to different tumor sites. The dimensions of the optical applicators and their irradiation patterns, the radiation wavelength, the thermal and optical properties of the tissue, the laser power and operating mode (continuous or pulsed), and duration of application are all factors affecting the size of the ablated site and the quality of the

outcomes. This means that the success of the treatment also depends on these factors and others like the real-time control of the temperature reached in the tumour, which is hardly predictable since the laser absorption by tissues depends on too many aspects. In LA, to measure local temperature variations, thermocouples or thermistors, available for other ablation treatments, can not be used since they are not easy to integrate in optical fibres and, being metallic, they interfere with the laser beam introducing artifacts. As an alternative, fibre optic sensors, such as Fibre Bragg Gratings (FBGs) sensors, can be used to perform real-time temperature measurements since they are transparent to the beam and they do not introduce relevant heat distribution perturbations.

Chapter 3

Introduction to laser devices, optical fibres and sensors

Since this thesis project focuses on laser ablation, the source used to produce tissue heating consists of a laser radiation, which is delivered to the target tissue through optical fibres. Optical fibres are also used to realize special sensors array based on FBGs, useful for measuring the temperature variations in different points of tissue during the heating phase of ablation.

This section provides at first a brief introduction to laser systems, to the mechanism of interaction between radiation and matter, and the general structural characteristics of a laser device. At the end, an introduction to optical fibres and FBGs is presented.

3.1 Introduction to laser systems

A LASER (acronym of Light Amplification by Stimulated Emission) is an optoelectronic system that produces a beam of coherent light thanks to a mechanism of interaction between light and matter called stimulated emission. The term "coherent" means that the generated beam has a fixed phase during its propagation, both in space and time. Laser radiations show also high irradiance, monochromaticity and allow obtaining devices that emit ultra-short pulses (order of femtosecond).

3.1.1 Radiation-matter mechanisms of interaction

The atoms are constituted by a nucleus, containing protons and neutrons, and surrounded by electrons. Electrons can only move at fixed distances from the nucleus, which correspond to fixed energy levels. The lower energy level, called fundamental state, corresponds to the minimal distance for the electron from the nucleus. When the electrons are excited, they can move from an internal level to an external one. Normally an excited electron tends to decay in random time, returning to its previous state with the emission of photons having energy equal to the energy difference between the excited state and the fundamental one. To better understand the radiation-matter interaction mechanisms we refer to a simplified atom in which electrons can occupy only two possible energy levels:

- The fundamental level, with energy E_1;
- The excited level, with energy E_2.

Three different mechanisms can occur in matter (Fig. 3.1):

- Absorption: by exciting the atom with an incident radiation, the incident photon is absorbed and its energy excites the electron from the E_1 state to the E_2 one;
- Spontaneous emission: an excited electron randomly decays from the upper energy level, emitting a photon with energy equal to the difference E_2-E_1;
- Stimulated emission: an incident photon stimulates the decay of an excited electron, resulting in the emission of another photon having the same characteristics (quantity of motion) of the incident one.

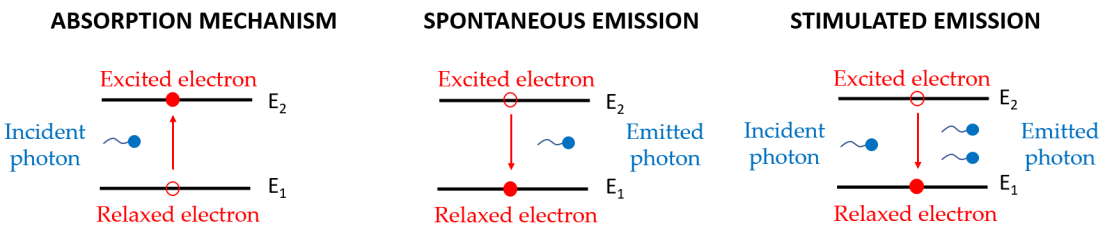

Figure 3.1: Absorption, spontaneous emission and stimulated emission mechanisms.

Laser devices rely on the stimulated emission to amplify light and, to have the stimulated emission prevailing over spontaneous emission, the population of the excited energy level must be larger than that of the fundamental level, a condition known as "population inversion". This can be obtained in the so-called "active materials" by providing a source of energy, called the "pump".

3.1.2 Architecture and principles of operation of LASER devices

Laser systems are made of three components:

- Active material;
- Pumping device;
- Optical resonator.

The active material is a gas, a solid or a liquid that, excited by a pumping device, produces photons by stimulated emission. It is contained in an optical resonant cavity formed two mirrors, one totally reflective and one partially reflective. In a simplified picture, photons bounce back and forth in the cavity, being amplified at each passage and occasionally leaving it through the partially reflecting mirror, thus originating the laser emission. The pump, which is the source of energy for the active medium, can be an optical (such as a flash lamp or another laser) or electrical source (Fig. 3.2).

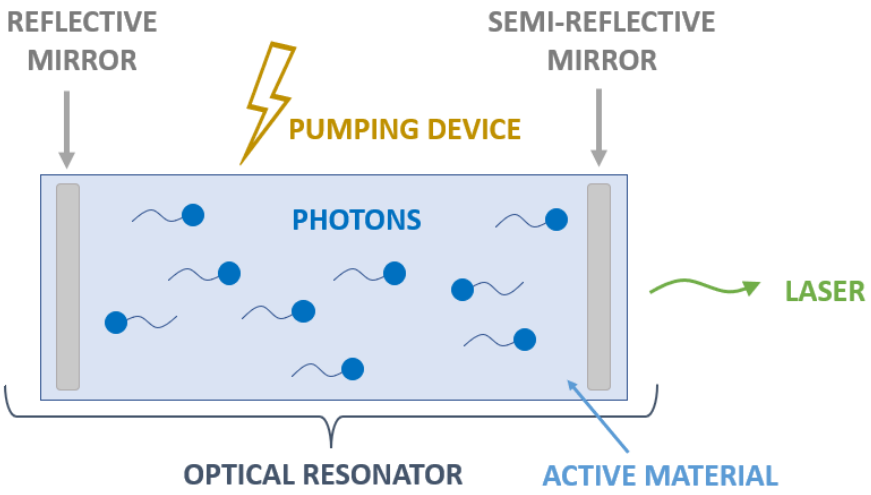

Figure 3.2: Structure of a laser.

To simply understand the phenomenon of generation of a laser radiation, we can imagine again that the electrons can occupy only the two levels of energies E_1 and E_2.

In *active materials* a *population inversion* is induced by the pumping mechanism. A population inversion occurs when most of the electrons constituting the atoms of the material are in the excited state rather than in the fundamental one, and remain in this condition for a relatively long time (of course, compared to the atomic time scale). In such conditions, when incoming photons of suitable energy hit the material, the phenomenon of stimulated emission can occur. In reality, stimulated emission, which is the origin of amplification in lasers, coexists with spontaneous emission, which is actually the mechanism that starts triggering the stimulated decay. However, for pump intensities above a certain limit value, called the "pump threshold", thanks to the effect of the optical cavity, stimulated emission prevails and the emission from a laser is beam with a high degree of coherence and brightness.

As already indicated, the previous discussion was a simplified explanation considering only two possible energy levels for electrons, which allows the simple understanding of the phenomena. However, it should be noted that two-levels lasers do not exist, and that actual laser require three or four energy levels, with the additional consideration of some meta-stable energy levels. An example is sketched in Fig. 3.3

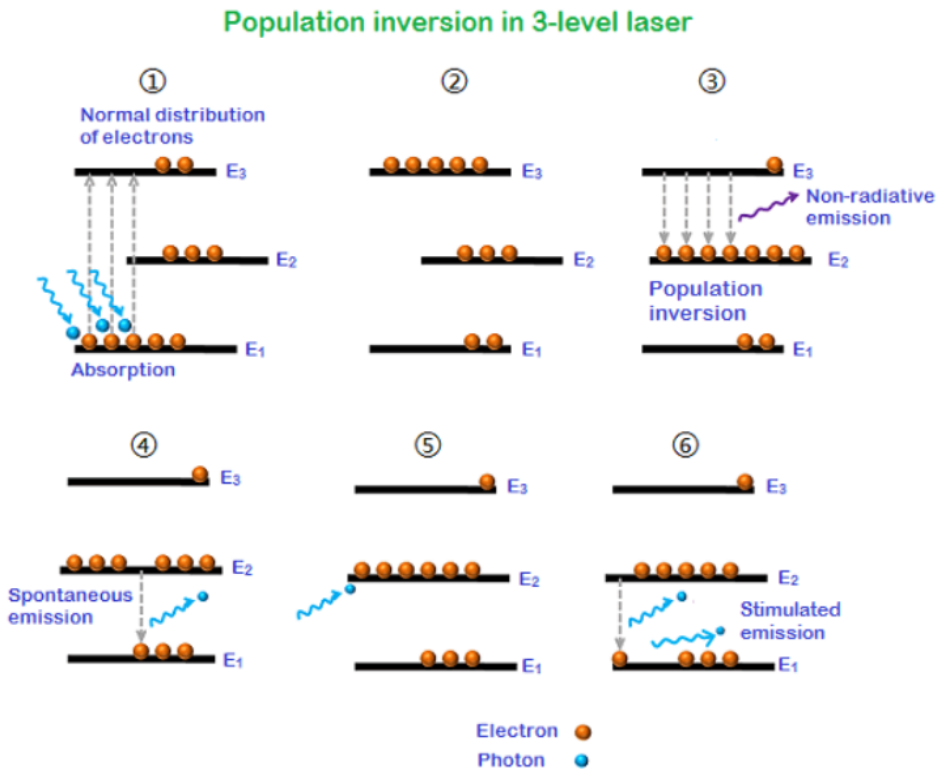

Figure 3.3: Three-levels laser [8].

3.1.3 Laser diode

A laser diode is an optoelectronic device consisting of a semiconductor crystal differently doped in two areas. In particular, it is made of a n-type region, with a high number of electrons, and a p-type region, poor in electrons. These regions are connected to two metal contacts. Between the two regions, an extra layer called *intrinsic layer* is inserted (Fig 3.4).

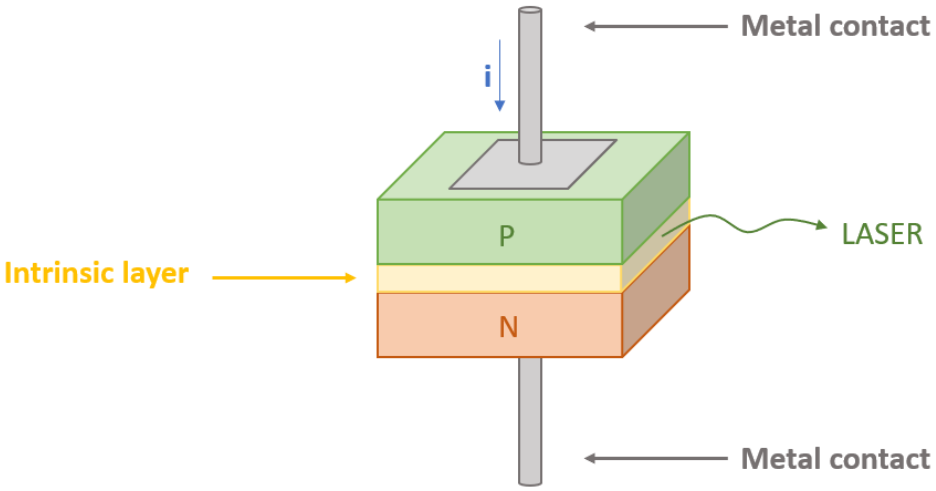

Figure 3.4: Structure of a laser diode.

Applying a potential difference by connecting the V+ terminal of a generator to the p-region and the V- terminal to the n-region (through metal contacts), the recombination between electrons and holes occurs, resulting in the generation of photons. Since in spontaneous recombination electrons and holes need time to recombine, it is possible that an already generate photon triggers the emission of another photon through the stimulated emission phenomenon. In a laser diode the recombination happens in the intrinsic layer, which is used as a light guide.

3.2 Introduction to optical fibres

Optical fibres are used to deliver the laser beam to the malignant lesion during an ablation procedure. An optical fibre is a small rod made of a combination of glassy and/or polymeric materials. In particular, we can distinguish an internal nucleus, called *core*, surrounded by the *cladding*, in turn covered by polymeric layers called *buffer* and *jacket*, which protect the fibre and improve the mechanical strength (Fig. 3.5).

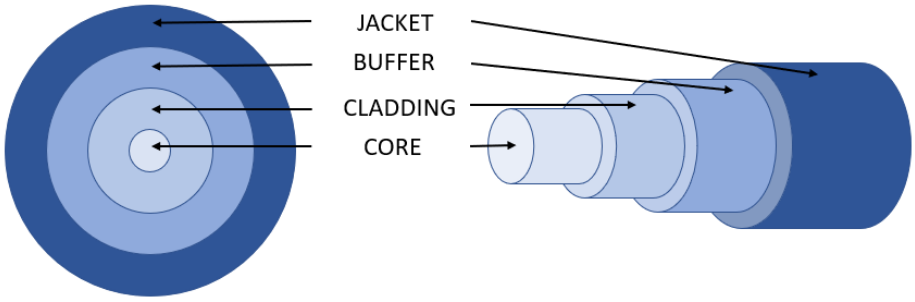

Figure 3.5: Schematic representation of the structure of an optical fibre.

Optical fibres rely on the total internal reflection at the core-cladding interface to confine light in the core. When a light ray hits a surface separating two media having different refractive index, it is partially reflected into the medium of origin and partially transmitted in the other medium (Fig. 3.6). The normal to the separation surface between the two media forms two angles with the incident ray and the transmitted ray, indicated respectively as α_1 and α_2.

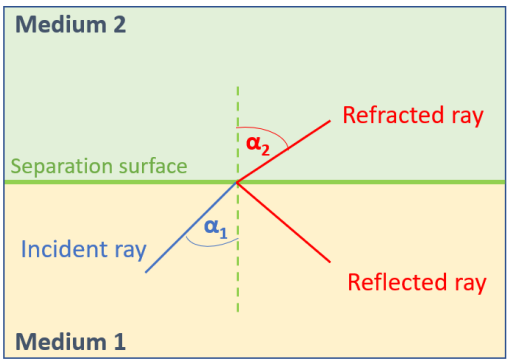

Figure 3.6: Schematic representation of the split of a light beam at the interface between two media with different optical properties.

These angles are related by the *Snell's law*:

$$n_1 \sin \alpha_1 = n_2 \sin \alpha_2 \tag{3.1}$$

where:

- n_1 is the refractive index of the first medium;
- n_2 is the refractive index of the second medium.

If $n_2 < n_1$, it exists a particular angle α_1, called *critical* or *limit* angle, for which $\alpha_2 = \frac{\Pi}{2}$. Above that incidence angle the incident ray is totally reflected and the total internal reflection condition is reached.

The same phenomenon is observable in an optical fibre and it is used to ensure the propagation of the light beam. Light propagation occurs into the core, because the refractive index of the cladding is lower than the refractive index of the core. This means that for specific incidence angle at the core-cladding interface the total reflection can occur. The angle of incidence at the separation surface in turn depends on the angle of the light entering the core. To ensure the total internal reflection, the light ray must enter into the core with a maximum angle θ (Fig. 3.7), which depends on a parameter called *Numerical Aperture* (NA). The NA is a dimensionless parameter that determines the angular limit within which the light propagation is guided in an optical fibre. A condition for the phase of the bouncing waves must also be met but, for large fibres as those used for laser ablation, the picture in terms of the NA is enough to explain the guidance of the light beams.

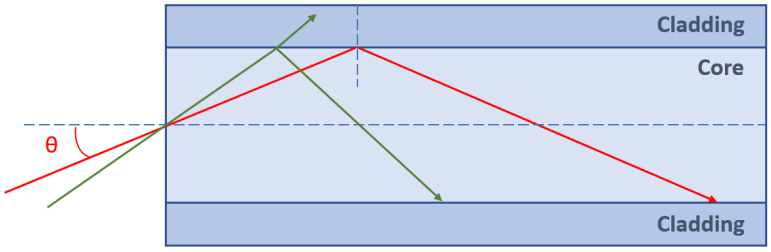

Figure 3.7: Propagation of light in an optical fibre.

Optical fibres can be classified into:

- *Single mode* optical fibres;
- *Multimode* optical fibres.

Single mode optical fibres like those used in telecommunications have a small core diameter (4 µm to 10 µm) while the diameter of the cladding is of 125 µm. Since the diameter of the core is small, the light beam passing through a single mode fibre propagates almost parallel to the axis of the fibre, so it exists a "single mode" of propagating. The core has a constant refraction index which rapidly decrease at the core-cladding separation surface, according to a step trend (Fig. 3.8). In this thesis single mode fibres have been used for sensing purposes.

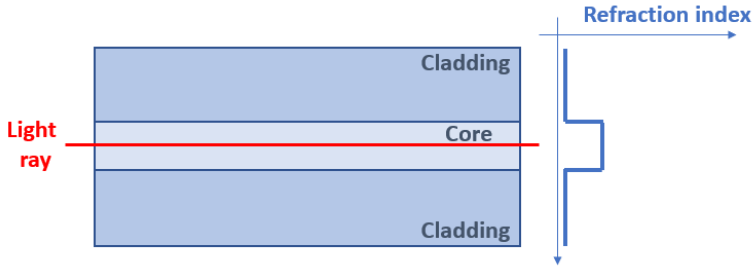

Figure 3.8: Propagation of light in a single mode fibre.

Multimode optical fibres have a larger core diameter (usually, for telecommunication applications 50 µm, with a cladding diameter always of 125 µm. In this case, the light passing through the fibre can propagate following different paths, which correspond to many modes. The refraction index between core and cladding can have a step trend like in single mode fibres or a profile that gradually decreases passing from the core to the cladding. Gradual decreasing profiles are used to limit the phenomenon of modal dispersion. The modal dispersion is the signal spreading in time due to the different propagation velocities of modes in the optical fibre (Fig. 3.9). The fibres used for laser ablation are multimode and characterized by a much larger core (and cladding) diameters that those typically used in telecommunications.

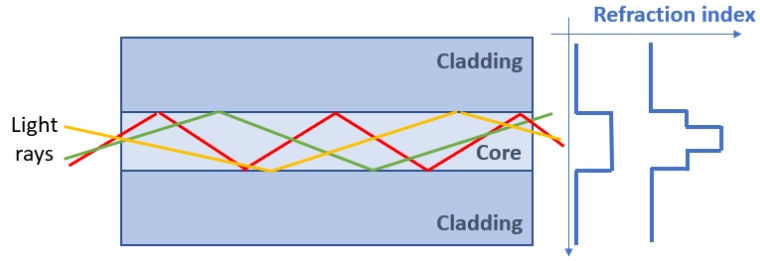

Figure 3.9: Propagation of light in a multimode fibre and examples of refractive index profiles.

3.3 Introduction to FBGs sensors

The Fibre Bragg Grating sensors are all-fibre devices obtained by inducing a periodic refractive index variation in the core of a single-mode optical fibre. Small size, high sensitivity, chemical inertia, immunity to electromagnetic interferences, biocompatibility and multiplexing capability are the main characteristics that have led, in recent years, to a growing interest in these sensors for possible applications in the medical field [9]. The modification of the refractive index results in a strongly spectral dependent behaviour of light propagation; in particular, when a broadband light propagates through the fibre, a narrow portion of the wavelengths centered around a specific wavelength, called the *Bragg Wavelength*, is reflected by the FBG while the rest of the spectrum continues to propagate along the fibre (Fig 3.10).

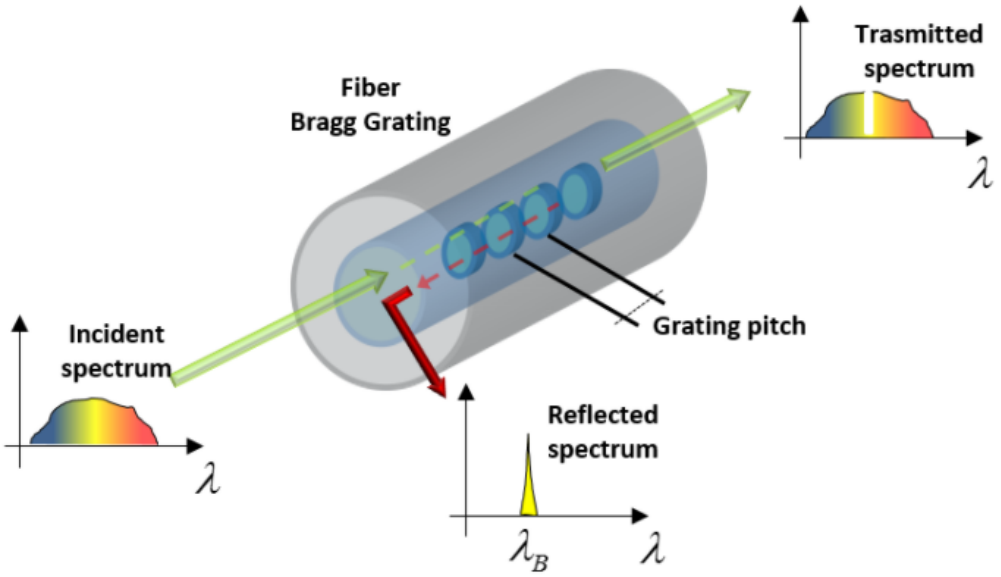

Figure 3.10: Incident and transmitted spectra of a Fiber Bragg Grating [10].

The Bragg wavelength is defined as:

$$\lambda_{\mathrm{B}} = 2n_{\mathrm{e}}\Lambda \tag{3.2}$$

where n_{e} is the effective refractive index and Λ is the FBG period.

The Bragg wavelength depends on temperature variations and strains (Fig. 3.11); indeed, its shift can be expressed as:

$$\Delta\lambda_{\mathrm{B}} = K_{\mathrm{T}}\Delta T + K_{\epsilon}\Delta\epsilon \tag{3.3}$$

where K_{T} is the *sensitivity to temperature* and K_{ϵ} is the *sensitivity to the strain*.

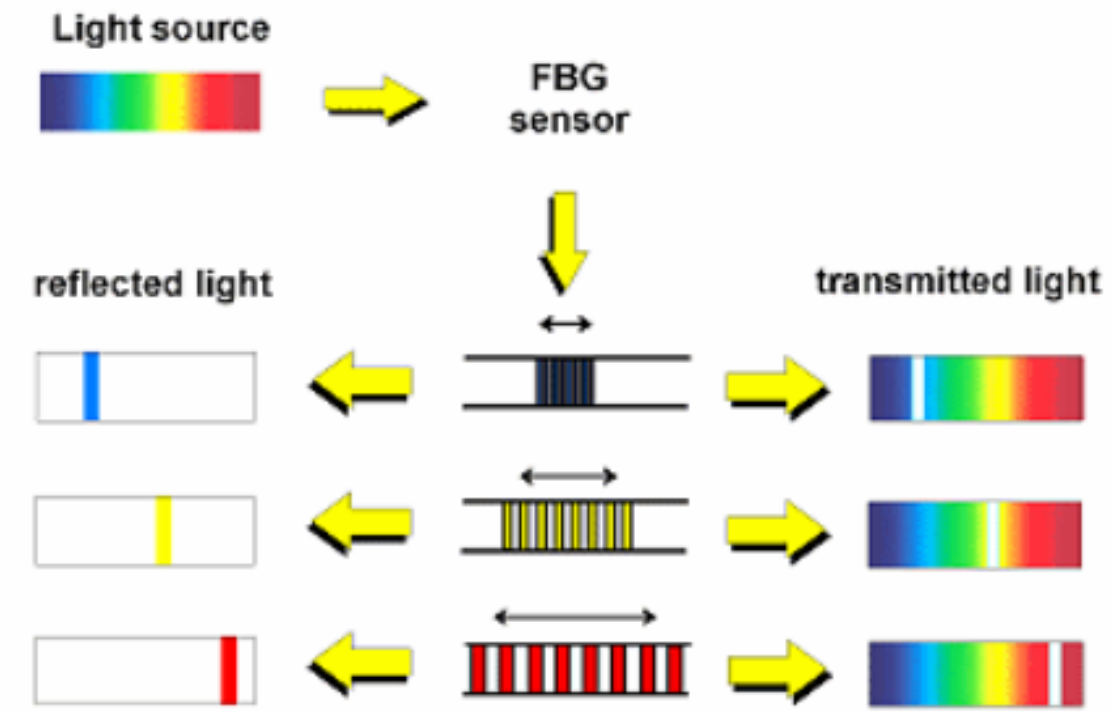

Figure 3.11: Bragg wavelength modification due to stimuli [11].

FBGs are manufactured different approaches:

- *Interferometric* technique [12]: this approach uses an UV laser beam, which is split in two rays by an interferometer; then, the two resulting beams are recombined after propagation through different optical paths to form an interference pattern (Fig. 3.12). The period of FBGs is equal to the period of the interference fringe pattern and it depends on the wavelengths of the incident rays and on the half-angle between the incident beams. This writing technique permits inscribing FBGs with Bragg wavelength at any wavelength but it has limited reproducibility due to the sensitivity to mechanical vibrations.

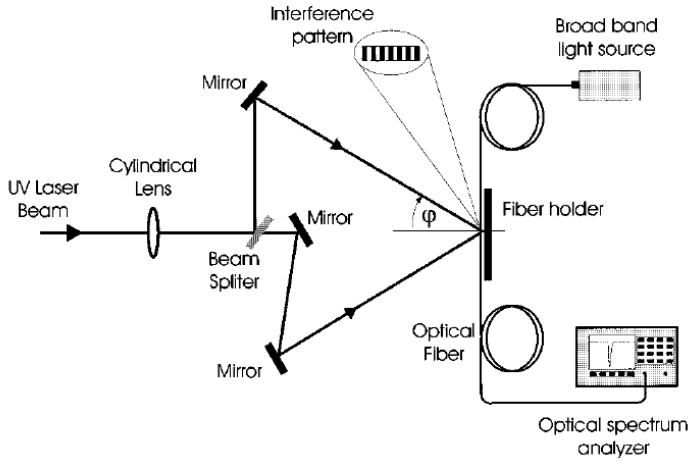

Figure 3.12: Interferometric fabrication technique [12].

- *Phase mask* technique [12]: a phase mask, which is a diffractive optical element, is used to inscribe FBGs inside the core. It is interposed between the UV writing ray and the fibre (Fig. 3.13). The mask can be obtained holographically or by electron-beam lithography. Sensitivity to mechanical vibrations is limited and complex patterns can be realised; the drawback is that FBGs with different Bragg wavelengths require different phase masks.

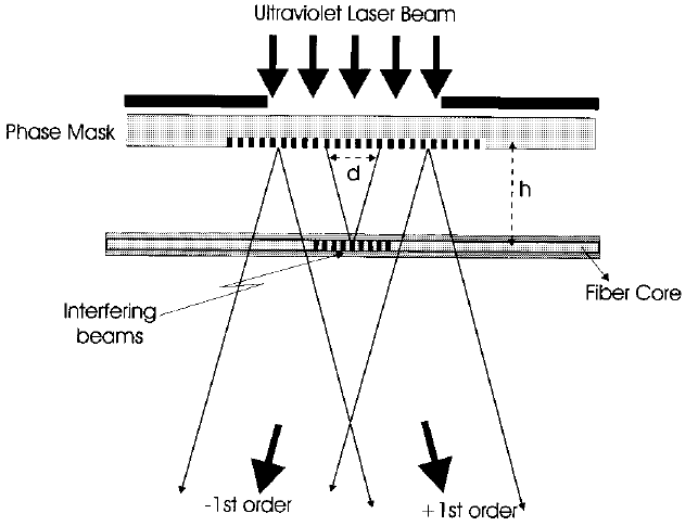

Figure 3.13: Phase mask technique [12].

- *Point-by-point* technique [12]: short pulses (typically obtained using a femtosecond laser) are used to change the refractive index of the core point by point (Fig. 3.14). The advantages are that writing wavelengths are not limited to UV and that complex induced refractive index patterns can be easily realised. In particular, the FBG sensors used for this thesis work have been fabricated using this approach.

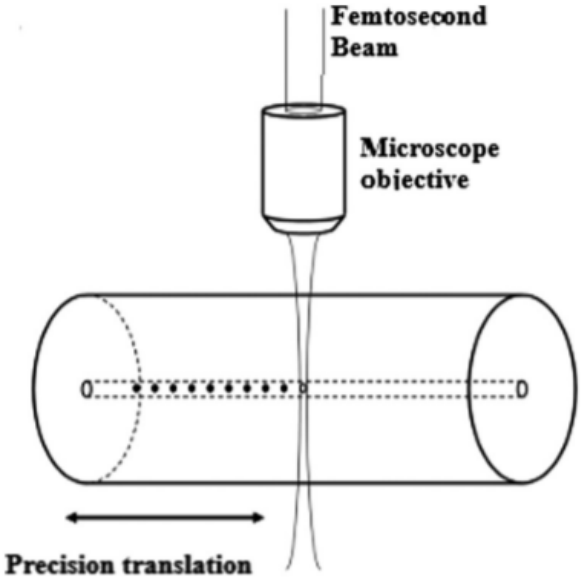

Figure 3.14: Point-by-point technique [13].

The FBGs can be classified according to their structure in (Fig.3.15) [9]:

– *Uniform* FBGs: they are the most common and the simplest configuration, in which the refractive index modulation has a constant period along the fibre axis. The reflected spectrum shows a peak centered in λ_B;

– *Chirped* FBGs: they are characterized of a non-uniform grating period, which usually increases with a linear dependence. It results in different λ_B being reflected from each portion of the FBG and in a wide reflected spectrum;

– *Blazed* or *Tilted* FBG: they show a constant grating period but the plane modulating the refractive index is not perpendicular to the fibre axis (tilted);

– *Etched* FBGs: the cladding of the fibre containing a uniform FBG is etched along the sensor;

– *Array* FBGs: they are made up of several FBGs inscribed into the same optical fibre. Each FBG reflects a different λ_B and therefore the reflected spectrum shows several peaks. They can be used for quasi-distributed sensing.

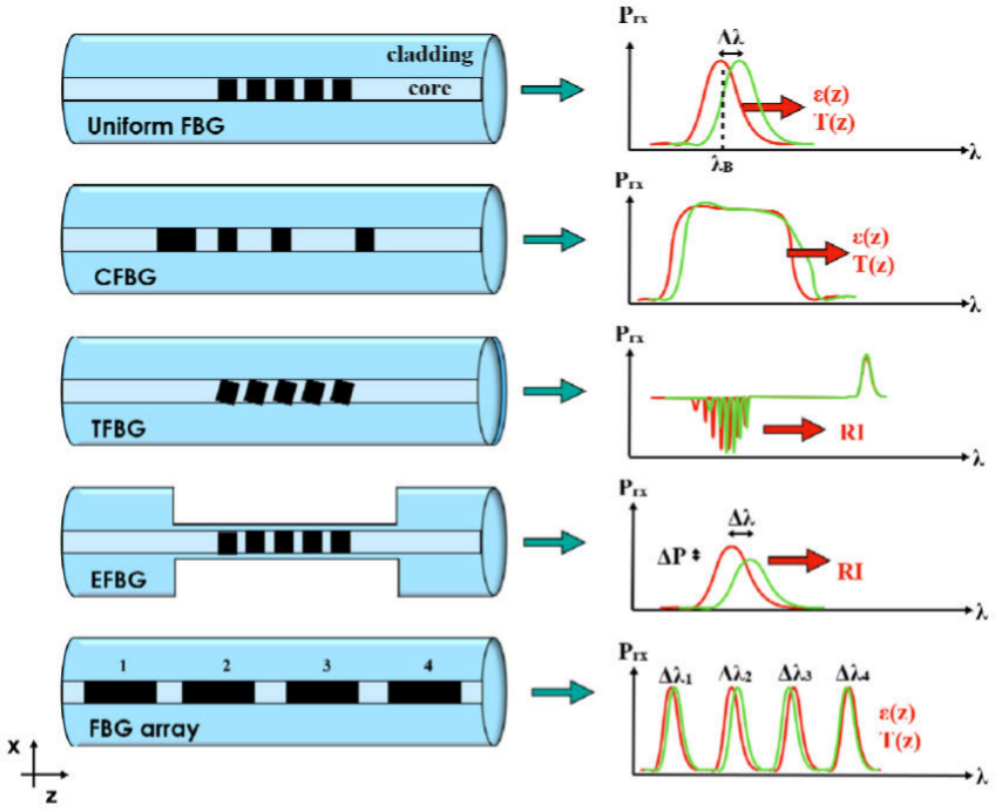

Figure 3.15: Uniform, chirped, tilted, etched and array FBG structures and spectral responses [9].

3.4 FBG interrogators

FBG interrogator is the generic name of instruments used to measure the shift of the Bragg wavelength over time. Different implementations are possible, all quite complicated and expensive because they must be able to detect wavelength variations in the order of 1 pm. In general, light from a suitable source is sent to the FBG sensor through a coupler or an optical circulator, which also routes the reflected signal to a receiver. Among the most common light sources there are the tunable laser and the broadband light source, such as a super-luminescent LED (SLED). Using a broadband light source requires a wavelength dependent receiver, such as an optical spectrum analyser (OSA), a spectrometer, or a power meter equipped with tunable pass-band optical filter. Instead, using a tunable laser source, a photodiode (followed by a trans-impedance amplifier to convert the output in a voltage) can be used for the receiver [14] (Fig. 3.16). The interrogator used in this thesis belongs to this category.

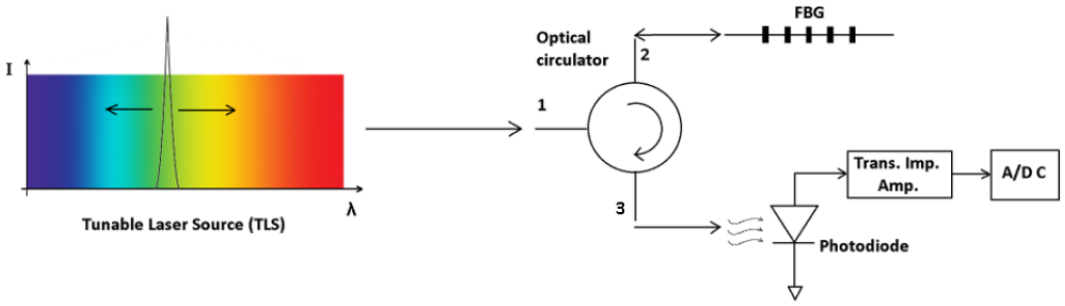

Figure 3.16: Principle of operation of a tunable laser source interrogator [14].

3.4.1 Micron Optics Hyperion si155

The interrogator used in this work for analyzing the reflected Bragg wavelengths from the FBG sensor arrays is the Micron Optics Hyperion si155, by Luna Technologies® (Fig. 3.17).

Figure 3.17: Micron Optics Hyperion si155, by Luna Technologies®.

The specifications of this optical interrogator are:

- range of wavelengths: 1,500 nm to 1,600 nm;
- resolution: 10 pm;
- maximum acquisition rate: 1 kHz;
- maximum number of parallel channels: 4.

An Ethernet line is necessary to remotely control the device. The include software, called *ENLIGHT Sensing Analysis*, permits the users to set data acquisition parameters, such as the acquisition rate or different thresholds for peaks detection (described in the following subsection), and to visualize in real-time the reflected peaks from the sensors connected to the channels. The Figure 3.18 shows its user interface.

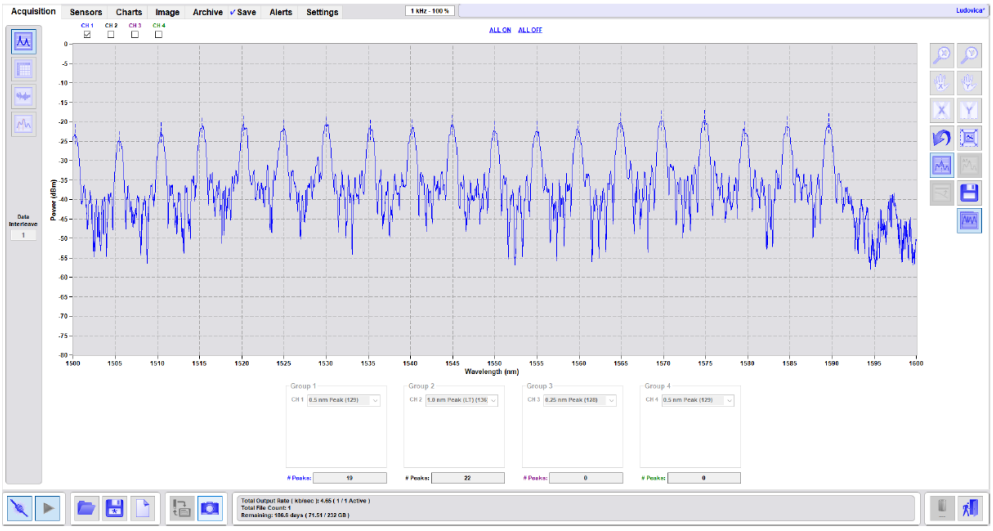

Figure 3.18: User interface [15].

Peak detection: the zero-crossing method

In order to detect the Bragg wavelength, the reflected signal is processed by the instrument. In particular, the reflected signal is at first filtered since it is affected by noise. The zero-crossing method is applied to the obtained profile. For this purpose, the filtered signal passes through a derivative filter and the zeros obtained are detected. According to this method, a single zero corresponding to the reflected Bragg wavelength should be obtained. Unfortunately, given the non-idealities of the reflected signal profile measured, it is possible to have more than a single zero. As a consequence, it necessary to impose a threshold value to correctly detect the Bragg Wavelengths.

Chapter 4

Fundamentals of heat conduction

This section briefly summarizes the fundamental concepts of heat transmission in solids, necessary for understanding the phenomena and methods described in the next chapter of this thesis. Fourier differential heat equation is introduced and the 3D Green's function is presented as an example of closed form solution of heat equation.

4.1 Heat conduction in solids

The heat propagation is a process of thermal energy transfer from media, or between parts of the same medium, at different temperatures. The driving force of the phenomenon is the difference of temperature. Heat transmission occurs in general according to the three mechanisms of conduction, convection and radiation. Even if the three phenomena often coexist, the prevalence of one of them over the others is observed depending on the media in which the heat transmission is taking place. In particular, conduction happens in solids, convection in liquid or aeriform, radiation in aeriform and in vacuum.
Heat conduction in a medium, in general, is a three dimensional and time dependent phenomenon based on two fundamental principles of classic physics:

- heat transfer always occurs from points at higher temperature to points at lower temperature;

- the storage of heat in a specific point of a body results in an increasing of temperature in that point, depending on the *specific heat capacity* of the body [16].

The heat problems can be classified as *steady-state* problems when the transient phase is ended, so the temperature does not change over the time, and *transient* or *unsteady-state* problems when it does.

4.2 Heat equation

The general equation describing the phenomena of heat conduction in a nonhomogeneous and anisotropic solid, is the partial differential *Fourier equation*:

$$c\rho\frac{\partial T}{\partial t} = \frac{\partial}{\partial x}\left(\lambda_x\frac{\partial T}{\partial x}\right) + \frac{\partial}{\partial y}\left(\lambda_y\frac{\partial T}{\partial y}\right) + \frac{\partial}{\partial z}\left(\lambda_z\frac{\partial T}{\partial z}\right) + Q \tag{4.1}$$

in which:

- c is the *specific heat capacity* ($\mathrm{J\,kg^{-1}\,K^{-1}}$);
- ρ is the *mass density* ($\mathrm{kg\,m^{-3}}$);
- λ_x, λ_y, λ_z are the *thermal conductivity* in the three directions ($\mathrm{W\,m^{-1}\,K^{-1}}$);
- Q is the *rate of internal heat generation* ($\mathrm{W\,m^{-3}}$)

If the medium is homogeneous the *thermal conductivity* does not depend on the point P(x,y,z). In case of isotropic media the *thermal conductivity* is the same in the three directions of space, so λ_x=λ_y=λ_z=λ.
Eq. 4.1 can be simplified in case of an homogeneous and isotropic media in:

$$c\rho\frac{\partial T}{\partial t} = \lambda\left(\frac{\partial^2 T}{\partial x^2} + \frac{\partial^2 T}{\partial y^2} + \frac{\partial^2 T}{\partial z^2}\right) + Q \tag{4.2}$$

Using the Laplacian differential operator

$$\nabla^2(\cdot) = \left(\frac{\partial^2(\cdot)}{\partial x^2} + \frac{\partial^2(\cdot)}{\partial y^2} + \frac{\partial^2(\cdot)}{\partial z^2}\right)$$

it can be written as:

$$c\rho\frac{\partial T}{\partial t} = \lambda\nabla^2 T + Q \tag{4.3}$$

In a stationary problem, Eq. 4.3 can be simplified into the *Poisson equation*:

$$\lambda\nabla^2 T + Q = 0 \tag{4.4}$$

If there is not heat generation inside the body, Eq. 4.3 can be simplified into the *diffusion equation*:

$$\frac{\partial T}{\partial t} = \alpha\nabla^2 T \tag{4.5}$$

where

$$\alpha = \frac{\lambda}{c\rho}$$

is the *thermal diffusivity* ($\mathrm{m^2\,s^{-1}}$).

In order to solve Eq. 4.3 an initial condition and some boundary conditions must be considered. The initial condition to be set defines the temperature of each point of the body at the starting heating propagation instant t=0. Since Eq. 4.3 is a first order differential equation in time, just one initial condition must be set. With respect to boundary conditions, the number of conditions necessary for each significant direction of propagation depends on the order of the differential equation in that direction. This means that if the heat conduction significantly takes places in one direction only, two boundary conditions must be considered, while for a 3D heat problem, six boundary conditions must be set [17].

Some examples of most common settable boundary conditions are:

- *Dirichlet conditions*: the temperature value at the surface of the medium is fixed;
- *Neumann conditions*: the heat flux through the surface of the medium is fixed;
- *Cauchy conditions*: temperature at the domain surface and heat flux through it are fixed.

4.3 The Green's function for heat equation

A Green's function, indicated as G, is the impulse response of a linear differential operator L applied on a domain with defined initial and boundary conditions. It means that it defines the behavior of a generic system when a pulse, a Dirac's delta function δ, occurs at its input and it is the solution of the equation:

$$L\,G = \delta \tag{4.6}$$

According to the heat equation the differential operator L is defined as:

$$\partial t - \alpha \nabla^2_{3D} \tag{4.7}$$

and G is a function of $r = r(x, y, z)$ and t:

$$G = G(x, y, z, t) = G(r, t) \tag{4.8}$$

In particular, the Green's function valid for a 3D heat conduction problem in a homogeneous and isotropic medium is the solution of the heat equation:

$$c\rho\frac{\partial T}{\partial t} = \lambda\nabla^2 T + \delta(t)\delta^3(x,y,z) \tag{4.9}$$

where the term $\delta(t)\delta^3(x,y,z)$ defines the impulsive source in space and in time. In particular, the solution is given by [18]:

$$G(r,t) = T(r,t) = \Theta(t)\Big(\frac{1}{4\pi\alpha t}\Big)^{\frac{3}{2}} \exp\Big(\frac{-r^2}{4\alpha t}\Big) \tag{4.10}$$

where:

- $\Theta(t)$ is the *Heaviside step function*;
- α is the *thermal diffusivity* of the medium.

The function $G(r,t) = T(r,t)$ defines the temperature value of each point of the medium with respect to time as a result of the application of the heat pulse to the system.

As the differential operator L is linear, knowing the response of a system to a pulse, it is possible to evaluate the response of the same system to any perturbation. The response $T'(r,t)$ of the system to a source function $x(r,t)$ different from the Dirac's delta function can be evaluated by convolution of the new input signal with the impulse response $G(r,t)$:

$$T'(r,t) = x(r,t) \circledast G(r,t) \tag{4.11}$$

Chapter 5

Thermal properties evaluation

This section provides an explanation of two possible methods for evaluating the tissue thermal parameters and a description of the thermal model created to validate one of them.

5.1 Thermal properties evaluation methods

Two thermal diffusivity evaluation methods have been developed:

- **First method** or **Green's function method (GF method)**
  It is based on the Green's function (described in Sect. 4.3):

$$T(t) = P\Big(\frac{1}{4\pi\alpha t}\Big)^{\frac{3}{2}} \exp\Big(\frac{-r^2}{4\alpha t}\Big) \tag{5.1}$$

  Multiplying by $t^{\frac{3}{2}}$ and applying the natural logarithm to both sides of the equation:

$$T(t)t^{\frac{3}{2}} = P\Big(\frac{1}{4\pi\alpha}\Big)^{\frac{3}{2}} \exp\Big(\frac{-r^2}{4\alpha t}\Big) \tag{5.2}$$

$$\ln\Big(T(t)t^{\frac{3}{2}}\Big) = \ln\Big(P\Big(\frac{1}{4\pi\alpha}\Big)^{\frac{3}{2}} \exp\Big(\frac{-r^2}{4\alpha}t\Big)\Big) \tag{5.3}$$

$$\ln\Big(T(t)t^{\frac{3}{2}}\Big) = \ln\Big(P\Big(\frac{1}{4\pi\alpha}\Big)^{\frac{3}{2}}\Big) - \frac{r^2}{4\alpha t} \tag{5.4}$$

By replacing: $z = 1/t$ and $f = \ln\left(T(t)t^{\frac{3}{2}}\right)$:

$$f = \ln\left(P\left(\frac{1}{4\pi\alpha}\right)^{\frac{3}{2}}\right) - \frac{r^2}{4\alpha}z \tag{5.5}$$

The function f obtained is a linear function in z. Its slope contains information on thermal diffusivity. Indicating the slope as

$$m = -\frac{r^2}{4\alpha}$$

the thermal diffusivity can be found as:

$$\alpha = -\frac{r^2}{4m}$$

- **Second method** or **Finite difference method (FD method)**
  The idea is to evaluate thermal diffusivity from the cooling curves of the tissue obtained experimentally. During the cooling phase there is not any heat source, so the heat equation describing the phenomenon is the diffusion equation:
  $$\frac{\partial T}{\partial t} = \alpha\nabla^2 T \tag{5.6}$$
  The diffusion equation can been solved using the *finite difference method*. The finite difference method is a strategy used to numerically solve differential equations based on the approximation of derivatives with finite difference equations. To use this method, it is necessary to know the temperature values in at least five points of the tissue, arranged as follows (Fig. 5.1):
  - a central node indicated as the (i, j) coordinates point;
  - two nodes horizontally aligned with the previous (i, j), the first on its left, the second on its right, respectively indicated as $(i-1, j)$ and $(i+1, j)$.
  - two nodes vertically aligned with the central (i, j), one above and the other below it, respectively indicated as $(i, j+1)$ and $(i, j-1)$.

  According to the finite difference method, the terms $\partial T/\partial t$ and $\nabla^2 T$ can be expressed as:

$$\frac{\partial T_{i,j}}{\partial t} = \frac{T_{i,j}(t_n + \Delta t) - T_{i,j}(t_n - \Delta t)}{2\Delta t}$$

$$\nabla^2 T_{i,j} = \frac{T_{i+1,j} - 2T_{i,j} + T_{i-1,j}}{\Delta x^2} + \frac{T_{i,j+1} - 2T_{i,j} + T_{i,j-1}}{\Delta y^2}$$

It means that the thermal diffusivity can be expressed as:

$$\alpha = \frac{\left(\frac{T_{i,j}(t_n + \Delta t) - T_{i,j}(t_n - \Delta t)}{2\Delta t}\right)}{\left(\frac{T_{i+1,j} - 2T_{i,j} + T_{i-1,j}}{\Delta x^2} + \frac{T_{i,j+1} - 2T_{i,j} + T_{i,j-1}}{\Delta y^2}\right)}$$

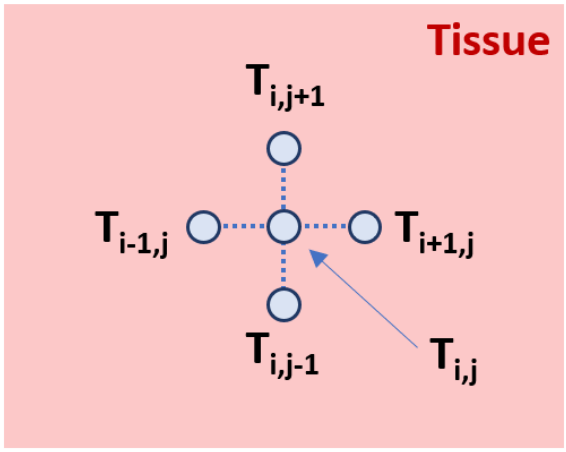

Figure 5.1: Position of five tissue points useful to evaluate thermal properties according to the second method.

Unfortunately, there are two limiting conditions to use this second method:

- the experimental measurements are affected by noise which complicates the calculation of second derivatives in the different directions of space;
- during the execution of the experimental tests, the alignment of five FBGs sensors useful for measuring the temperatures at five points of the tissue according to the described geometry is not simple, since they are not visible.

For these reasons, in this thesis project the first method described has been used to obtain information on thermal diffusivity of the tissue. To validate the method, a thermal model on MATLAB® has been developed.

5.2 Thermal model

A thermal model is a mathematical model that allows representing, more or less faithfully, a natural thermal phenomenon. In this thesis, a thermal model has been created in MATLAB® to validate the method, based on the Green's function, used to evaluate the thermal diffusivity of the tissue. The Partial Differential Equation (PDE) toolbox, which provides functions to solve the heat problem using the Finite Element Method (FEM) analysis, has been used. FEM is a numerical technique used to solve complex problems described by partial differential equations by reducing the latter to algebraic equations. The method is based on a discretization of the domain to be analyzed in many sub-domains of elementary form, called as *finite elements*. The discretization is achieved by creating a grid, called *mesh*. The elementary forms could be one-dimensional, two-dimensional or three-dimensional depending on the geometry characteristics and they are connected through *nodes*. The discritization determines the transformation of a continuous domain, with an infinite number of unknowns, into a discrete domain with a finite number of unknowns, simpler to solve. The approximation of the solution depends on the number and size of the finite elements: the finer is the discretization, the better is the accuracy of the solution. However, a finer discretization requires a higher computational cost.

The model developed in MATLAB® reproduces the phenomenon of heating of a homogeneous and infinite medium due to a point heat source inside it.
The *createpde* function has been used to create a transient thermal model. A 2D-domain has been constructed as a square of side 20 mm.
The impulsive source in space and time was modeled using the *internalHeatSource* function. To generate a pulse source in space another square of side 0.1 mm has been created at the centre of the domain (Fig. 5.2).

To simulate a pulse over time, the created area has been transformed into a $1{,}000\,\mathrm{W\,m^{-1}}$ heat source for a time of 0.01 s. To discretize the domain, a mesh grid made of 11.589 nodes has been created with the *generateMesh* function (Fig. 5.3).

The thermal properties have been assigned to the model using the *thermalProperties* function. In particular, the following parameters have been set:

- Thermal conductivity $\lambda = 1\,\mathrm{W\,m^{-1}\,K^{-1}}$;
- Specific heat $c = 1\,\mathrm{J\,kg^{-1}\,K^{-1}}$
- Mass density $\rho = 1\,\mathrm{kg\,m^{-2}}$

These thermal parameters are not realistic since the purpose of the model created is not to simulate the real phenomena of heat propagation in the tissue but to validate the method based on the Green's function described.

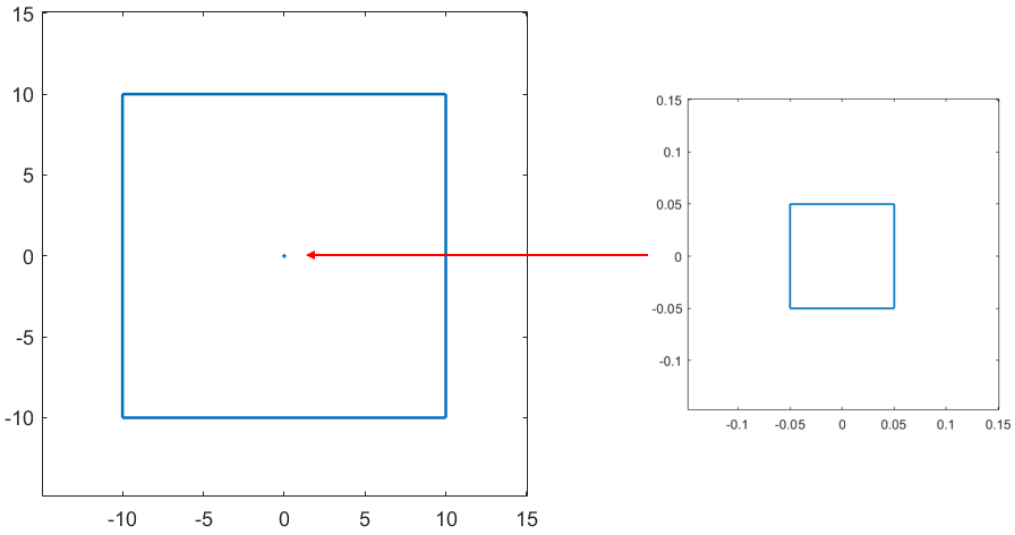

Figure 5.2: Geometry of domain and internal heat source.

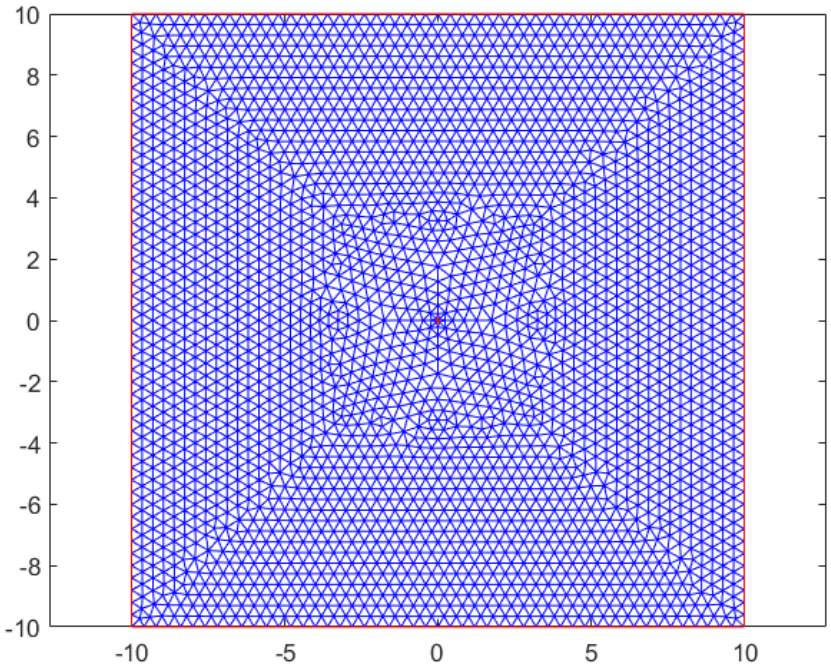

Figure 5.3: Mesh grid created inside the domain.

Before starting the simulation, initial conditions and boundary conditions has been set as follows:

- Initial temperature $T_0 = 0\,°\text{C}$;
- Temperature at each edge of the domain $T_\text{B} = 0\,°\text{C}$.

Using the *solve* function, the heat equation has been solved.

The simulated solution and the analytical one (temperature variations functions) have been compared at different nodes of the grid. The solutions proved to be comparable at grid points located in an intermediate area between the source and the edges of the domain (Fig. 5.4). At the points closest to the source the solutions are quite different due to numerical errors. The same happens at the boundaries, since the solution is affected by boundary conditions.

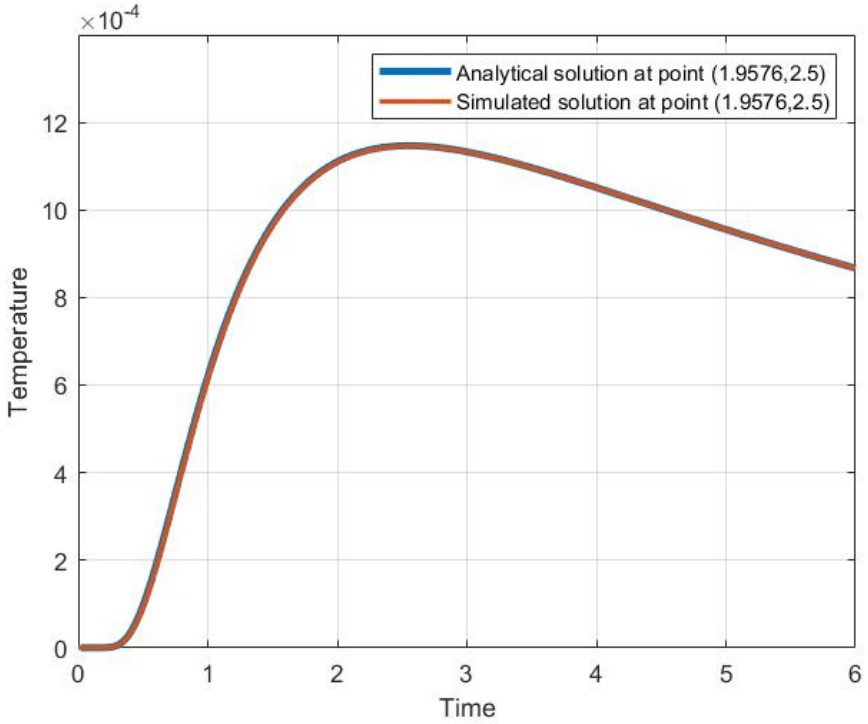

Figure 5.4: Analytical and simulated solution compared at the node (1.9576,2.5).

Considering the (analytical and simulated) solutions in a point of the domain in which they are comparable, by substituting one of them to the $T(t)$ term in equation 5.1 and proceeding as explained in paragraph 5.1 of this thesis, the thermal diffusivity has been obtained. The fitting was done using the *polyfit* and *polyval* functions of MATLAB®. The thermal diffusivity value obtained was found equal to the expected one ($1\,\mathrm{m^2\,s^{-1}}$), with an error of 0.1%. This way, the method has been validated.

Chapter 6

Experimental activities

This section provides an introduction to the instrumentation used to perform the heating tests on ex-vivo bovine tissue, the experimental set-up and the data processing methods used to evaluate thermal parameters from experimental temperature curves measured.

6.1 Instrumentation

The following tools were used to perform the heating tests:

- LASER device;
- MicronOptics HYPERION si155 interrogator (described in Sect. 3.4.1);
- Delivery fibre;
- FBGs-based temperature sensor arrays.

6.1.1 Laser device

The device used to induce tissue heating (Fig. 6.1) is based on a laser diode. It is equipped with:

- an *on/off switch* located at the back of the device;
- a *display* through which the user can choose the irradiation settings;
- a *pedal* to start/stop the irradiation;
- a *safety key* that protects the users from unwanted switching on of the laser. The key must be turned to start irradiation;

- an *emergency stop button* to immediately stop irradiating in case of danger.

Figure 6.1: Laser device.

After turning on the device, the display shows an interface (Fig. 6.2) to set:

- the emission wavelength: 915 nm or 1,470 nm;
- the emission power;
- the emission modality: continuous wave (CW) or pulsed wave (PW);
- the frequency and the Duty Cycle (DC) in case of PW emission modality;
- the emission time control: manual (through a pedal and a chronometer) or automatic (timer).

After setting these parameters and pressing the confirmation button, a summary of the chosen irradiation mode is shown and a safety warning appears, providing an additional level of control. After turning the key, the safety warning can be closed and irradiation can start.

Figure 6.2: Laser display.

6.1.2 FBG temperature sensor arrays

To measure the induced temperature variations, three Fibre Optic Sensor (FOS) quasi-distributed sensors have been used. Each sensor is an array of 20 multiplexed FBGs, inscribed in the core of a standard single-mode fibre (core diameter about 10 µm and cladding diameter of 125 µm). Their specifications are:

- *First array*, indicated as *"A1"*
  - length of each FBG: 1 mm;
  - FBGs arranged along two parallel axes;
  - distance between two consecutive sensors (of different axes): 1 mm;
  - Bragg wavelength range: 1,500 nm to 1,595 nm
  - Bragg wavelength difference between two consecutive sensors: 5 nm
- *Second array*, indicated as *"A2"*
  - length of each FBG: 1 mm;
  - FBGs arranged along two parallel axes;
  - distance between two consecutive sensors (of different axes): 1 mm;
  - Bragg wavelength range: 1,500 nm to 1,595 nm;
  - Bragg wavelength difference between two consecutive sensors: 5 nm

- *Third array*, indicated as *"A3"*
  - length of each FBG: 1 mm;
  - FBGs arranged along two parallel axes;
  - distance between two consecutive sensors (of different axes): 1 mm;
  - Bragg wavelength range: 1,505 nm to 1,600 nm;
  - Bragg wavelength difference between two consecutive sensors: 5 nm.

Table 6.1 summarizes their specifications.

Array	Bragg Wavelength [nm]	Number of sensors	Distance [mm]
A1	1500-1595	20	1
A2	1500-1595	20	1
A3	1505-1600	20	1

Table 6.1: Details of the arrays.

FBGs Characterization

The relation between the temperature and the Bragg wavelength reflected from each FBG is:

$$\lambda_{\mathrm{B}} = \lambda_0 + K_{\mathrm{T}} t \tag{6.1}$$

in which:

- λ_{B} is the Bragg wavelength (nm);
- λ_0 is the Bragg wavelength at $T = 0\,^{\circ}\mathrm{C}$ (nm);
- K_{T} is the temperature sensitivity ($\mathrm{pm}\,^{\circ}\mathrm{C}^{-1}$);
- T is the temperature value (°C).

In order to transform the Bragg wavelengths into temperature values, λ_0 and K_T must be known. These values can be obtained performing the characterization of the sensors.

For the activity described in this thesis it is necessary to measure the temperature variations in different tissue points rather than the absolute temperature values. By replacing the λ_0 with the first wavelength λ_S measured by the optical interrogator at the beginning of the tests for each FBG, these temperature variations can be evaluated. This is the reason why the term λ_0 is not necessary.
Furthermore in other thesis works it has been verified that, for these sensors, the value of K_T is approximately equal to $10\,\mathrm{pm}\,^{\circ}\mathrm{C}^{-1}$. For this reason, the three sensor arrays used in this thesis have not been fully characterized.

6.2 Experimental set-up

The experimental tests have been conducted on a workbench equipped with the optical interrogator and the computer.

On the desk, an acetate sheet was fixed and a slice of ex-vivo bovine liver tissue was positioned on it. The acetate sheet had not a central role in the measurements, it has been used just to avoid soiling the table and the instrumentation.
On the liver slice FBGs sensor arrays and the delivery fibre have been positioned according to different geometric arrangements, depending on the type of test. All the fibres have been also fixed at the table using the scotch tape in order to limit their movements, trying not to introduce strain, which would be detected by the sensor as temperature variations.
To simulate the insertion of fibres into the organ, another slice of tissue was placed on top of the first one, covering all the fibres carefully and avoiding, as far as possible, their displacement.
The delivery fibre has been connected to the laser device and all the sensor arrays to the optical interrogator (Fig 6.3).

In the end, the power of laser beam has been set and the acquisition data has been started. The irradiation time has been chosen by setting a timer or controlled by pedal after starting the laser device. After irradiating, the cooling phase data were also acquired. The data is acquired using the ENLIGHT software provided by Micron Optics, the manufacturer of the interrogator. At the end of the test, data acquisition has been stopped.

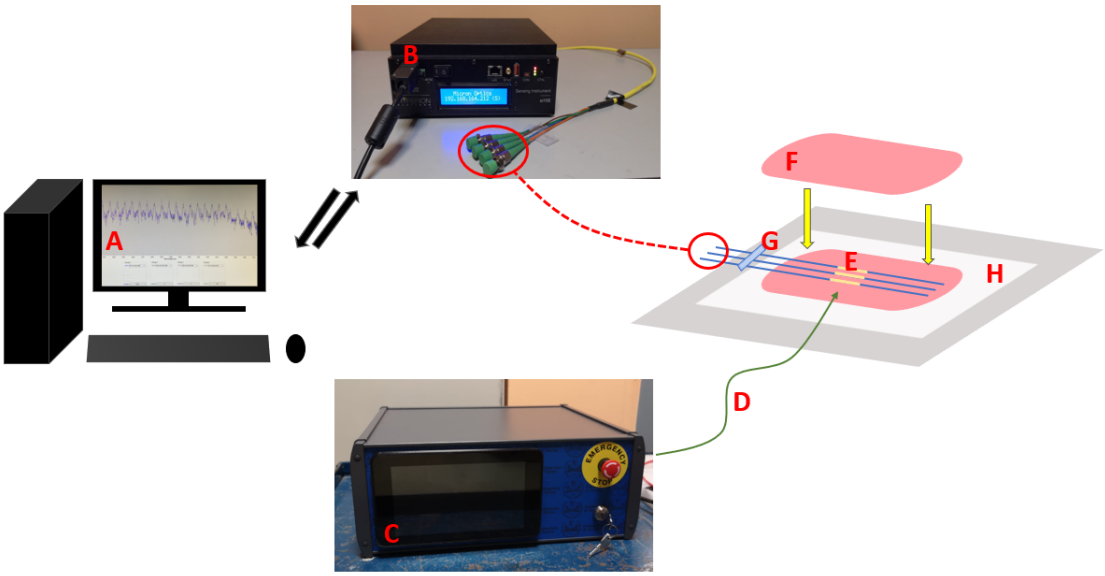

Figure 6.3: Schematic representation of the experimental setup: A) ENLIGHT software - B) MicronOptics interrogator - C) Laser device - D) Delivery fibre - E) FBGs sensor arrays - F) Slice of tissue - G) Scotch tape - H) Acetate sheet.

6.3 Data processing

After executing the tests (performed as described in Sect. 6.2), the acquired data file has been saved and processed. In particular, for each test, the values of the wavelengths reflected by each FBG have been transformed into temperature values according to the equation:

$$T = \frac{\lambda_B - \lambda_S}{K_T} \tag{6.2}$$

λ_S is the first Bragg wavelength measured by the optical interrogator at the beginning of the test. This means that the temperatures evaluated are actually temperature variations with respect to the initial temperature value. For each sensors array used, 20 temperature variation curves have been obtained over time (Fig. 6.4).
The *"central"* sensor, meaning the closest to the source, has been defined as the one that measured the maximum temperature change during the test (Fig. 6.5). The curves obtained from the measurements made by the sensors closest to the source have been considered for evaluating thermal properties (Fig. 6.6).

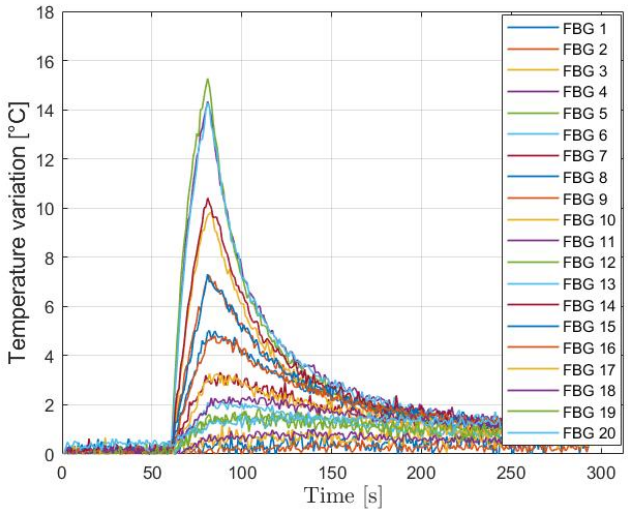

Figure 6.4: Example of a temperature functions obtained from the wavelengths reflected from all the FBGs of an array.

In particular, the 9 central sensors have been considered. Since the sensors are spaced 1 mm, 8 mm along the direction of the array have been examined. The data from other sensors, being further away from the source, have not been used since the measured temperature variations appeared comparable to the background noise present in each measure.

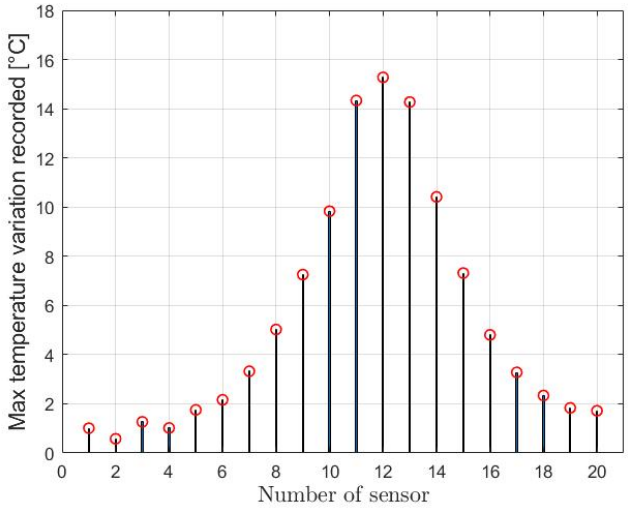

Figure 6.5: Example of maximum temperatures recorded graphic used to find the *"central"* sensor.

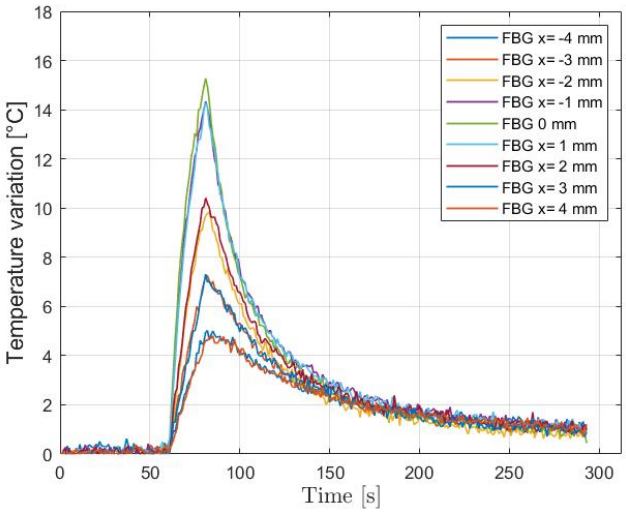

Figure 6.6: Example of temperature functions obtained from the central sensors of the array.

The experimental temperature functions obtained have been used to calculate thermal diffusivity values according to the Green's function method (*"first method"*) described in Sect. 5.1.

The Green's function, as previously explained, is the impulse response. The laser source used experimentally has been turned on for at least 20 seconds during the tests. The intent was to find a compromise between an excessive heating, which would have caused a change in the properties of the tissue, and a heating not detectable by the sensors. For this reason, the laser source used can not be considered as an impulse source in time. Furthermore, it can not even be considered a Dirac's delta in space.

In order to apply the method, two different strategies have been applied:

- the thermal properties have been evaluated considering the cooling phase of the tissue only, starting from the maximum temperature variation recorded. This permits to imagine that, before cooling, a pulse source have generated the temperature variation, leading the tissue to the maximum value of temperature recorded;

- the thermal properties have been evaluated considering the heating phase after having convoluted the real source with the impulse response. The response of the system to the real source has been found by applying the convolution between the real input signal to the system and its impulse response.

These two methods for calculating thermal diffusivity will be indicated from now on as *"cooling method"* and *"heating method"*. The next sections of this thesis describe the main details.

6.3.1 Cooling method

Since the Green's function depends also on the heating phase, the times vector to be multiplied for the experimental temperature function (as in Eq. 5.2) needed to be modified. For this purpose, it has been imagined to apply a pulse centered in the center of gravity of the actual heating phase performed. The initial cooling time T_{C} has been set as:

$$T_{\mathrm{C}} = \frac{T_{\mathrm{MAX}} - T_{\mathrm{START}}}{2} \tag{6.3}$$

where;

- T_{MAX} is the maximum temperature variation detected;
- T_{START} is the initial heating time.

The cooling is considered finished when the temperature variation returns to be smaller than 1 °C. The last part of the cooling phase (corresponding to the temperature variation between 1 °C and 0 °C) has not been considered as the noise excessively hides the useful signal.

A MATLAB® code has been developed to obtain the thermal diffusivity values from the data recorded by each FBG, according to the procedure described in section 5.1. Actually, the calculation procedure followed has been slightly modified. The modification has been made since the experimental data obtained from the $ln(T(t)t^{\frac{3}{2}})$ term did not follow a linear trend, but a parabolic one. It has been suggested that, since the thickness of the tissue slices is not infinite, there could be energy losses due to their interfaces with the air and the workbench. To consider these possible energy losses, a loss factor term βt has been add to the Green's function. Similarly to the description in 5.1, the modified procedure is:

$$T(t) = P\Big(\frac{1}{4\pi\alpha t}\Big)^{\frac{3}{2}} \exp\Big(\frac{-r^2}{4\alpha t} - \beta t\Big) \tag{6.4}$$

Multiplying by $t^{\frac{3}{2}}$ and applying the natural logarithm to both sides of the equation gives:

$$T(t)t^{\frac{3}{2}} = P\Big(\frac{1}{4\pi\alpha}\Big)^{\frac{3}{2}} \exp\Big(\frac{-r^2}{4\alpha t} - \beta t\Big) \tag{6.5}$$

$$\ln\left(T(t)t^{\frac{3}{2}}\right) = \ln\left(P\left(\frac{1}{4\pi\alpha}\right)^{\frac{3}{2}}\exp\left(\frac{-r^2}{4\alpha t} - \beta t\right)\right) \tag{6.6}$$

$$\ln\left(T(t)t^{\frac{3}{2}}\right) = \ln\left(P\left(\frac{1}{4\pi\alpha}\right)^{\frac{3}{2}}\right) - \frac{r^2}{4\alpha t} - \beta t \tag{6.7}$$

By replacing $z = 1/t$ and $f = \ln\left(T(t)t^{\frac{3}{2}}\right)$:

$$f = \ln\left(P\left(\frac{1}{4\pi\alpha}\right)^{\frac{3}{2}}\right) - \frac{r^2}{4\alpha}z - \frac{\beta}{z} \tag{6.8}$$

By multiplying by z both sides:

$$g = fz = \ln\left(P\left(\frac{1}{4\pi\alpha}\right)^{\frac{3}{2}}\right)z - \frac{r^2}{4\alpha}z^2 - \beta \tag{6.9}$$

The best fit to the data points have been found using the *polyfit* and *polyval* functions of MATLAB® (Fig. 6.7). In this case, indicating with m the leading coefficient of the quadratic equation, thermal diffusivity values have been calculated as:

$$\alpha = -\frac{r^2}{4m}$$

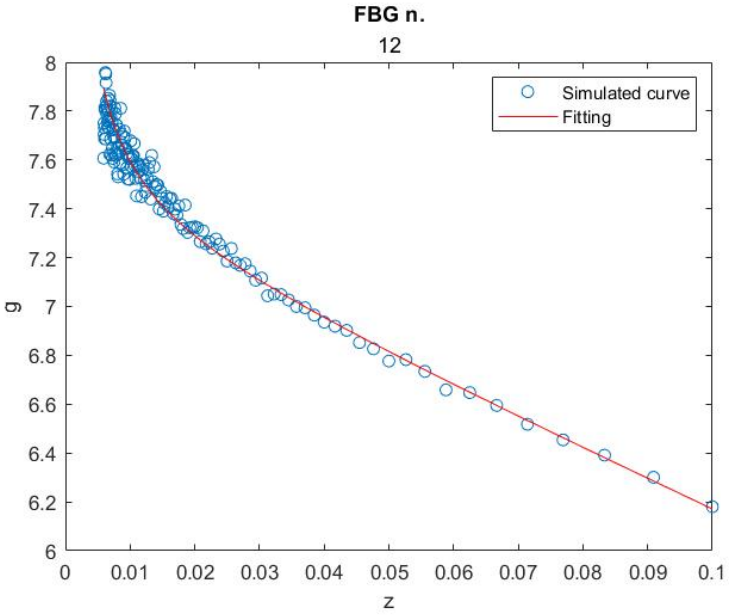

Figure 6.7: Example of a curve fit obtained.

6.3.2 Heating method

A method has been developed to evaluate thermal properties from the acquired heating phase data. As previously explained, the real laser source used experimentally is not considerable as a Dirac's delta in time, since it emits for a not infinitesimal time. Moreover, it has also a distribution in space. It means it can not be considered a point source in space.

The response of the system to a similar source is unknown, but it can be found by computing the convolution integral of the actual source function entering the system $x'(r,t)$ with the Green's function:

$$T(r,t) = x'(r,t) \circledast G(r,t) \tag{6.10}$$

For this purpose the actual source function has been modeled as a rectangular function in time and a Gaussian distributed source in space.

The rectangular function has been chosen imagine that the actual source emits a constant power during its working.

Since the source distribution in space is unknown, the Gaussian distribution represents a hypothesis made in order to simplify the mathematical calculations.

In this case, the equation to be solved is:

$$c\rho\frac{\partial T}{\partial t} = \lambda\nabla^2 T + \delta(t)\delta^3(r) \tag{6.11}$$

During switching on the source (in $[0, t*]$ time interval):

- $\delta(t) = Q$;
- $\delta^3(r) = \left(\frac{1}{2\pi\sigma_S^2}\right)^{\frac{3}{2}} exp\left(\frac{-r^2}{2\sigma_S^2}\right)$

The system response to the new source $x'(r,t)$ can be calculated as:

$$T(r,t) = x'(r,t) \circledast G(r,t) = Q\Big(\frac{1}{2\pi\sigma_S^2}\Big)^{\frac{3}{2}} \exp\Big(\frac{-r^2}{2\sigma_S^2}\Big) \circledast \Big(\frac{1}{4\pi\alpha t}\Big)^{\frac{3}{2}} \exp\Big(\frac{-r^2}{4\alpha t}\Big) \tag{6.12}$$

By replacing ${\sigma_t}^2 = 2\alpha t$ it gives:

$$T(r,t) = Q\Big(\frac{1}{2\pi\sigma_S^2}\Big)^{\frac{3}{2}} \exp\Big(\frac{-r^2}{2\sigma_S^2}\Big) \circledast \Big(\frac{1}{2\pi {\sigma_t}^2}\Big)^{\frac{3}{2}} \exp\Big(\frac{-r^2}{2{\sigma_t}^2}\Big) \tag{6.13}$$

Using the *fminsearch* function of MATLAB® the difference between the analytical solution and the experimental heating curves recorded has been minimized. Figure 6.8 shows the best fit of the nine heating curves recorded from central sensors.

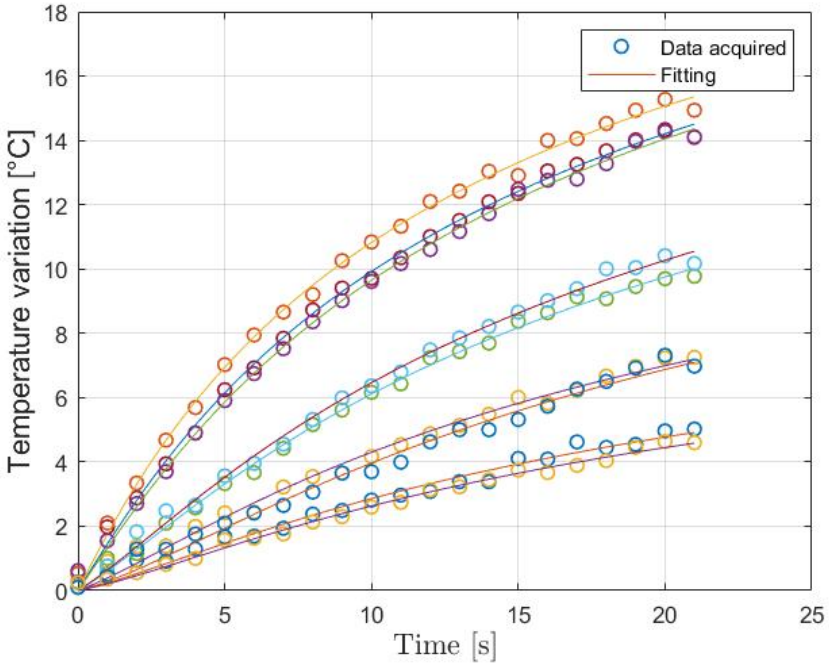

Figure 6.8: Best fit of the heating curves.

The thermal diffusivity values are calculated considering the optimization parameter returned by the *fminsearch* MATLAB® function.

Figure 6.9 summarizes the described data processing methods that can be use to evaluate the tissue thermal properties.

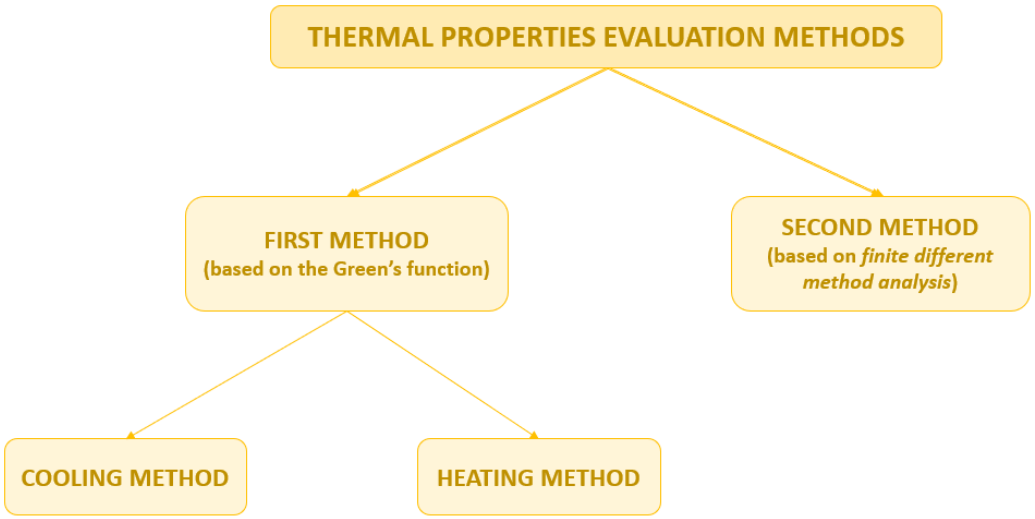

Figure 6.9: Data processing methods.

Chapter 7

Tests details and results

Some tests have been performed using different laser powers, irradiation times and fibres placements between the tissue slices. This section provides the specifications of the tests executed proceeding as described in section 6.2 and the results obtained following the data processing methods described in section 6.3.

7.1 Tests and results

All tests have been performed on slices of ex-vivo bovine tissue having a thickness of approximately 4 mm. The delivery fibre and sensor arrays have been placed on the liver tissue slices according to two different arrangements. From now on, they will be indicated as *"first configuration"* and *"second configuration"*.

7.1.1 First configuration tests

Some heating tests have been performed placing the three sensor arrays (A1, A2 and A3) and the delivery fibre on the first slice of tissue as indicated:

- The delivery fibre has been positioned on the tissue slice;
- A1, A2 and A3 arrays have been placed in a direction perpendicular to the delivery probe. The details of the arrays placement are:
  - A1 placed at 2 mm apart from the source end;
  - A2 placed at 1 mm apart from A1, it means 3 mm from the source end;
  - A3 placed at 1 mm from A2 and 4 mm from the source end.

Figure 7.1 shows the placement of the fibres.

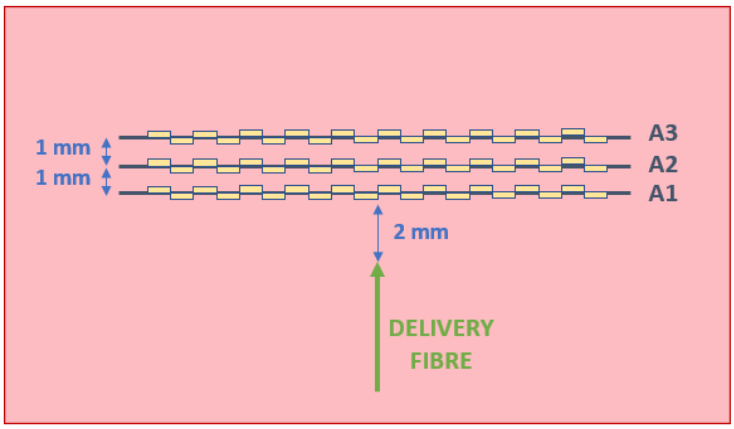

(a) *Schematic representation of the fibres distribution on tissue.*

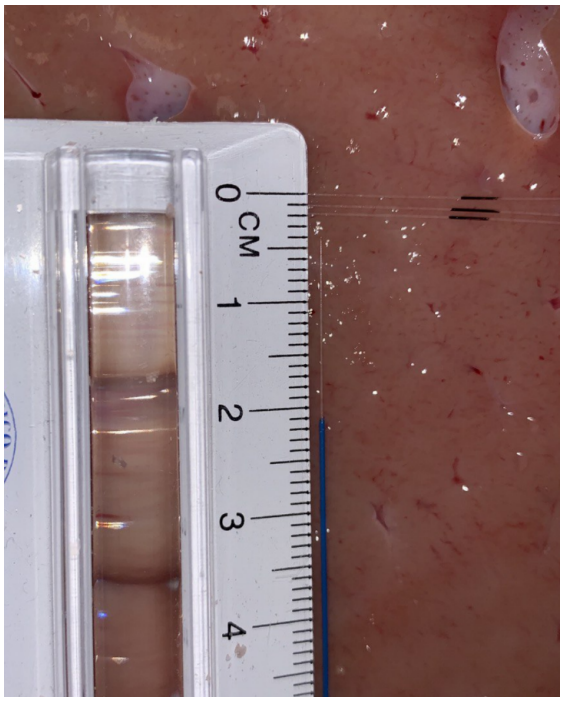

(b) *Detail of the distances between fibres on real tissue.*

Figure 7.1: Fibres placement on ex-bovine tissue slice.

Six tests have been carried out using this fibres placement. They have been performed moving the fibres arrangement in three different areas of the same liver tissue slice, maintaining the described geometry. Table 7.1 summarizes the tests details. Tests performed in the same location of the tissue are indicated with the same "Area of tissue slice"number.

Test number	Area of tissue slice	Power [W]	Irradiation time [s]
1	1	2	20
2	1	3	20
3	2	2	25
4	2	3	25
5	3	2	25
6	3	3	25

Table 7.1: Details of the tests.

7.1.2 Second configuration tests

The alignment of the sensing fibres while performing the previous tests proved to be complicated. In fact, placing the second slice of liver tissue over the delivery fibre and the sensing fibres to "simulate" their introduction inside the organ could compromise the geometric alignment. For this reason, in order to minimize the fibres movements when covering them, other tests have been performed fixing the fibres with tape on an acetate sheet. In particular, a "rectangular window" has been cut out from the acetate sheet, the sensor arrays and the end of the delivery fibre have been placed inside it and fixed with tape on the frame (Fig. 7.2).

In addition, these tests have been performed placing the fibres according to a different geometric arrangement (Fig. 7.3):

- The delivery fibre has been positioned on the tissue slice;
- A1 has been placed in the direction perpendicular to the delivery fibre, at a distance of 2 mm from its end;
- A2 and A3 have been positioned along the direction parallel to the delivery fibre, respectively 2 mm on its right and 2 mm on its left.

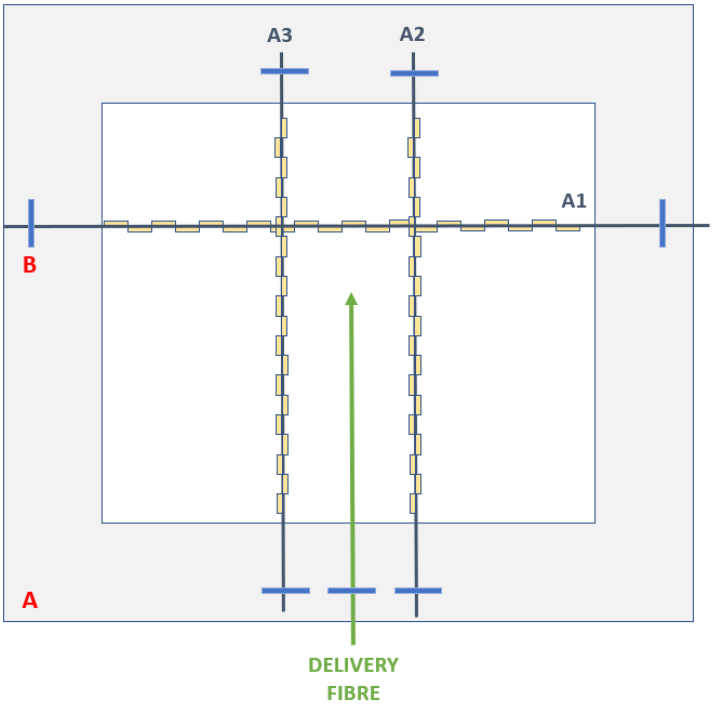

Figure 7.2: Fixing of fibres on the acetate sheet. A) Acetate sheet - B) Tape.

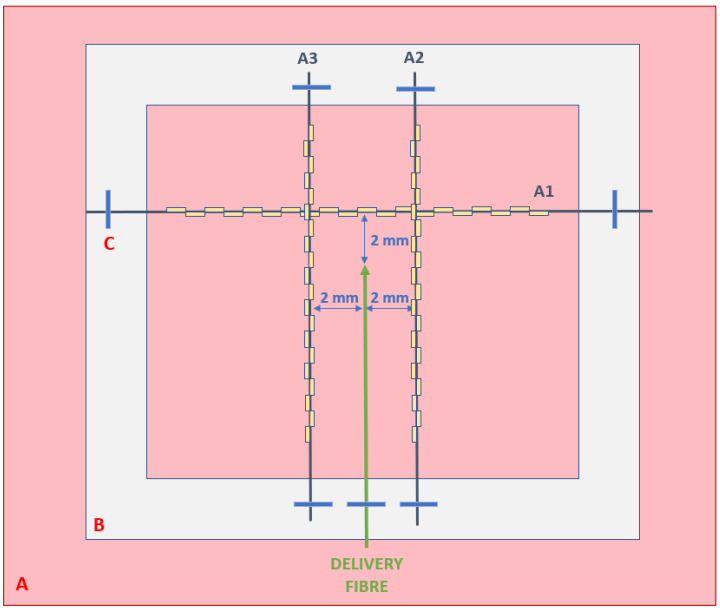

Figure 7.3: Schematic representation of the fibres configuration on tissue. A) Liver tissue - B) Acetate sheet - C) Tape.

Six tests have been carried out in this case. They have been performed placing the acetate sheet, with the fibres on it, in three different locations of the same liver tissue slice. Table 7.2 summarizes the details of the tests. Tests performed in the same position are indicated with the same "Area of tissue slice" number.

Test number	Area of tissue slice	Power [W]	Irradiation time [s]
1	1	2.5	40
2	1	2.5	40
3	2	2.5	40
4	2	3	40
5	3	3	40
6	3	3	40

Table 7.2: Details of the tests.

7.2 Results

This section shows the results obtained from the data acquired in all tests, processed as described:

- the data acquired from the first configuration tests and second configuration tests have been both processed using the cooling method.
  The sections 7.2.1 and 7.2.2 show the results of these analyses and the Figure 7.4 summarizes the methods used to obtain them.

- the data acquired from the second configuration tests have also been processed according to the heating method. The results are shown in section 7.2.3. The Figure 7.5 summarizes the methods used to obtain them.

.

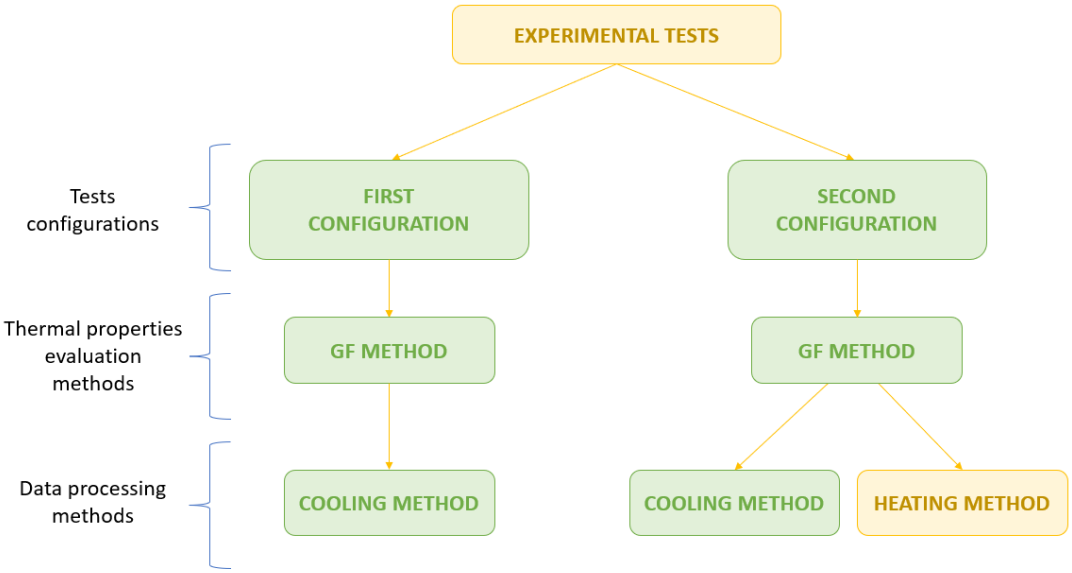

Figure 7.4: Highlighted in green the path followed to obtain results showed in sections 7.2.1 and 7.2.2.

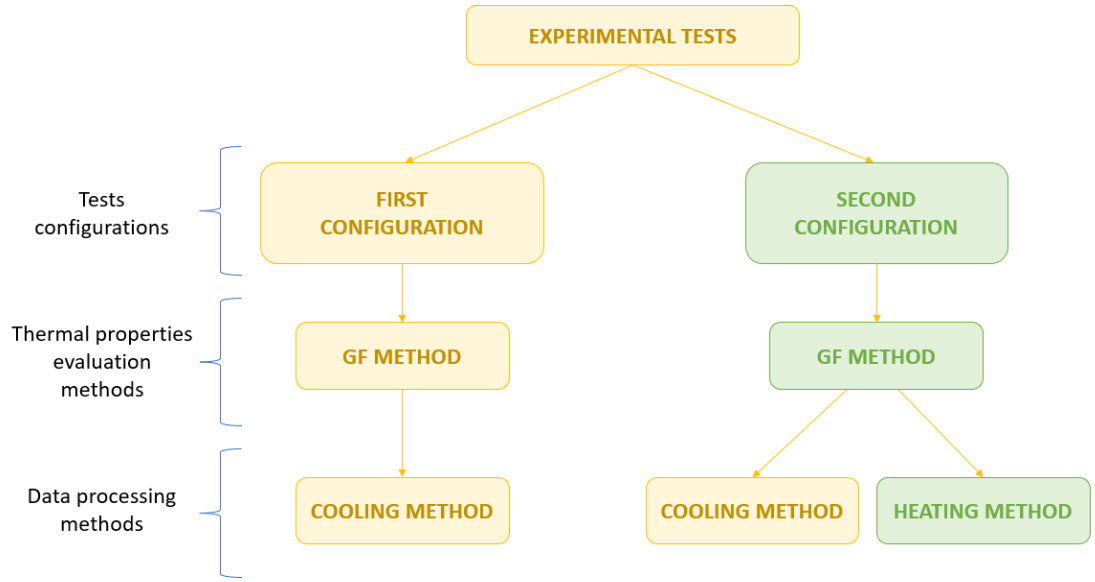

Figure 7.5: Highlighted in green the path followed to obtain results showed in sections 7.2.3.

In all the figures showed in the following sections of results, the abscissas report the distances of each considered sensor from the source. This distance should not be interpreted as the radial distance from the delivery fibre end. A coordinates system, whose origin corresponds to the end of the delivery fibre, has been considered for both fibres configurations (Fig. 7.6, 7.7). According to these coordinates systems, the distance of each sensor is expressed as the distance between the sensor itself and the axis of the coordinates system perpendicular to the array direction to which the sensor belong.

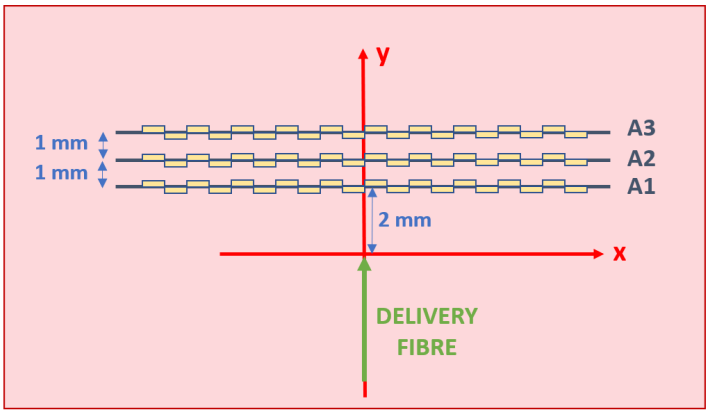

Figure 7.6: x-y coordinate system for calculating sensor distances from the source.

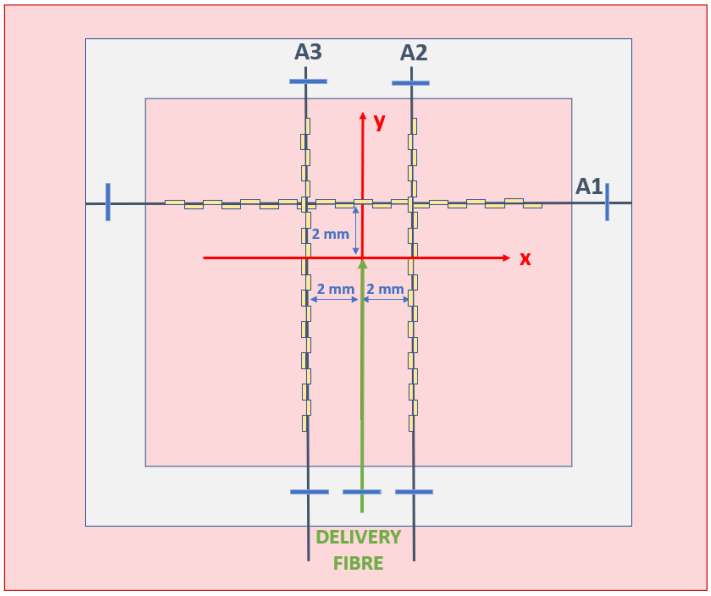

Figure 7.7: x-y coordinate system for calculating sensor distances from the source.

More simply, the abscissas report:

- the distances between each sensor and the y-axis of the coordinates system for arrays placed in a perpendicular directions with respect to the delivery fibre direction;

- the distances between each sensor and the x-axis of the coordinates system for arrays parallel to the delivery fibers direction;

7.2.1 The cooling method - First configuration tests

The figures 7.8, 7.9 and 7.10 show the thermal diffusivity values obtained from the data acquired from sensors closer to the source of each array (respectively A1, A2 and A3) in all the tests performed with first fibres configuration.
In all graphics, the abscissas report the distances of each sensor from the delivery fibre direction along the direction of the considered array.

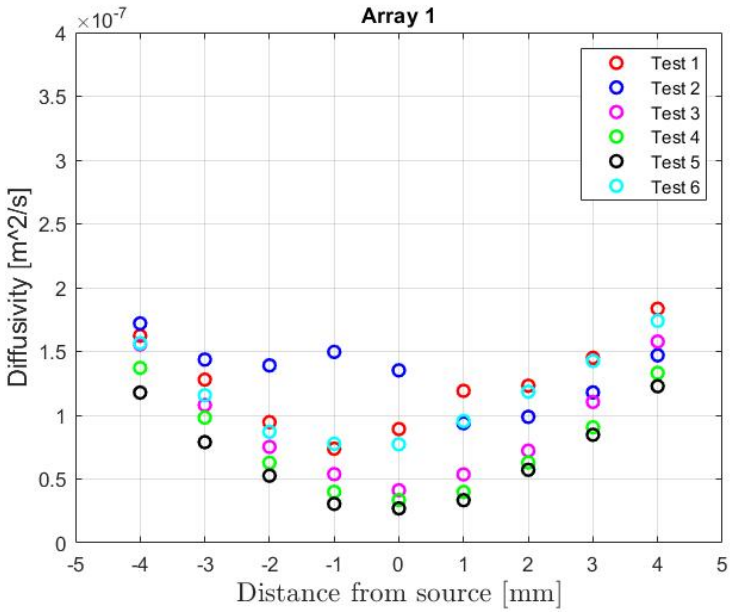

Figure 7.8: Diffusivity values obtained from data measured by sensors of *"first array (A1)"*.

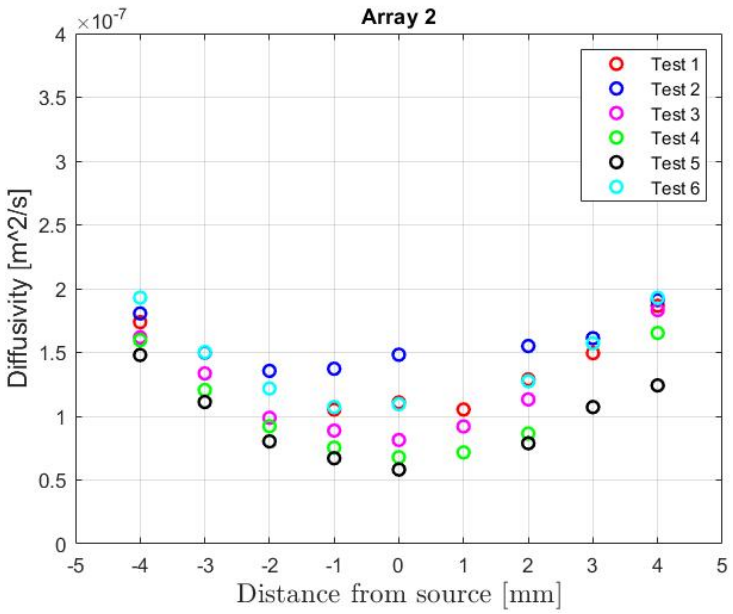

Figure 7.9: Diffusivity values obtained from data measured by sensors of *"second array (A2)"*.

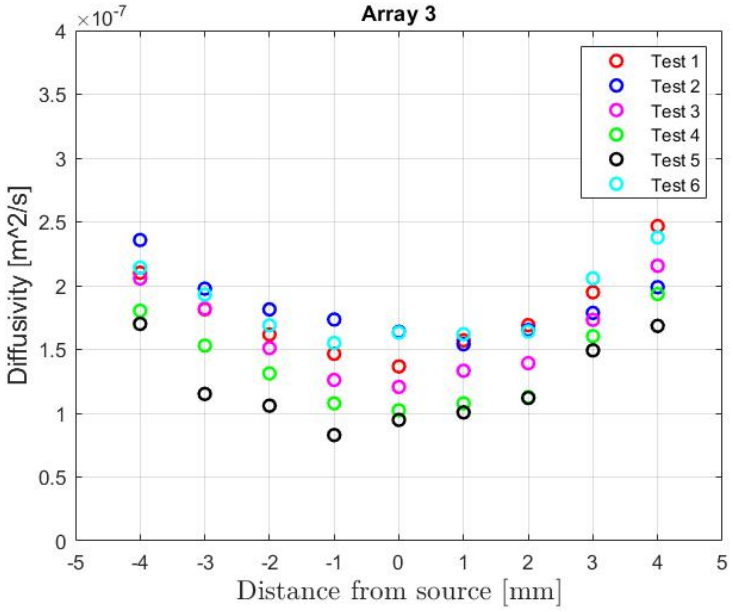

Figure 7.10: Diffusivity values obtained from data measured by sensors of *"third array (A3)"*.

Considerations on results

It is possible to notice that the values obtained processing the data acquired from each FBG show a parabolic trend over the distance and all the thermal diffusivity values are in the range $0.02\,\mathrm{mm^2\,s^{-1}}$ to $0.25\,\mathrm{mm^2\,s^{-1}}$. The variability of the values obtained from all FBGs in different tests could be a consequence of the displacement of the arrays while covering them with the second tissue slice.

7.2.2 The cooling method - Second configuration tests

The figures 7.11, 7.12 and 7.13 show the thermal diffusivity values obtained from the data acquired from sensors of each array (respectively A1, A2 and A3) in all the tests performed with second fibres configuration. In particular, data the nine sensors closer to the source have been considered for each array. As previously explained, the abscissa in figure 7.11 reports the x-distances of each sensor from the y-axis of the coordinates system considered. The abscissa in figures 7.12 and 7.13 reports instead the y-distances of each sensor from the x-axis of the coordinates system (Fig. 7.7).

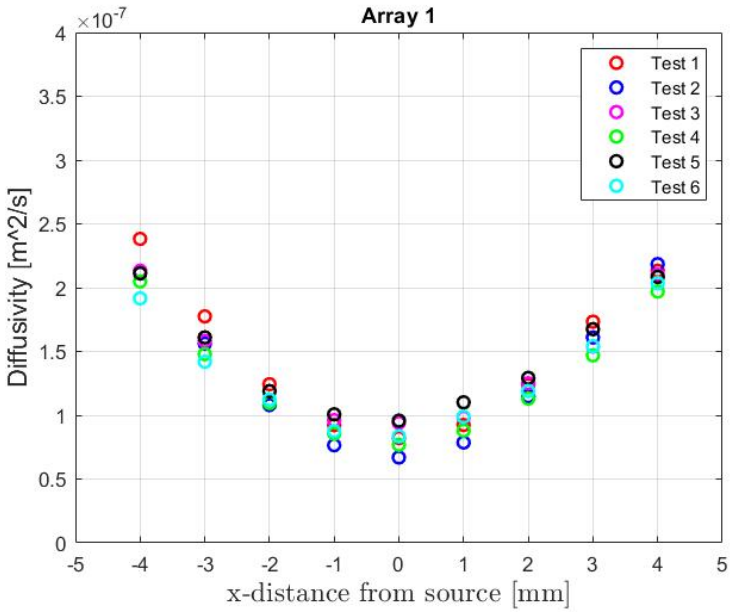

Figure 7.11: Diffusivity values obtained from data measured by sensors of *"first array (A1)"*.

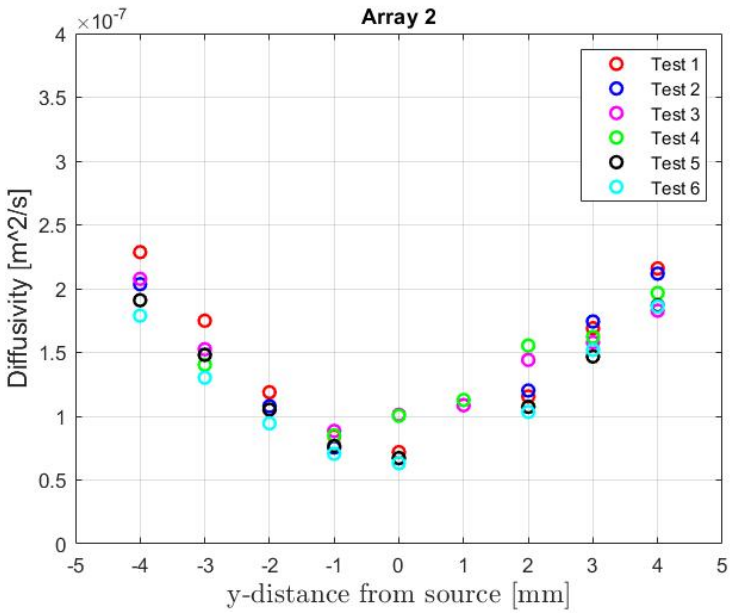

Figure 7.12: Diffusivity values obtained from data measured by sensors of *"second array (A2)"*.

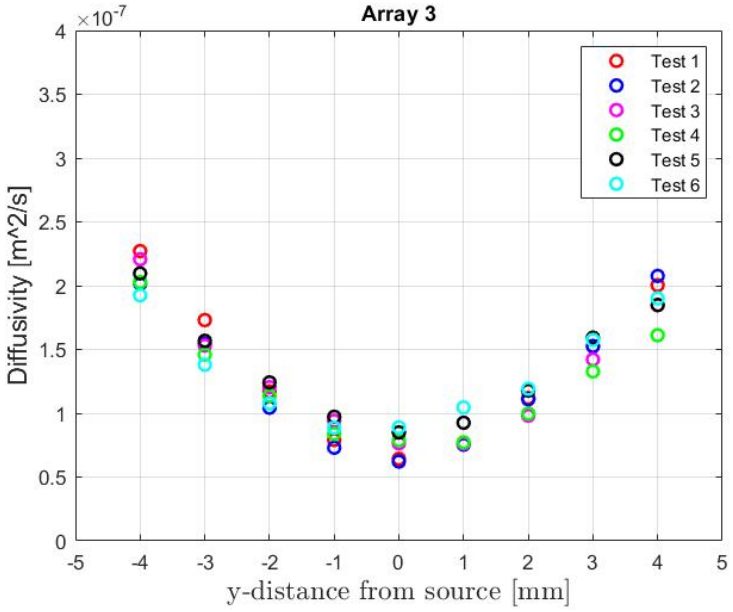

Figure 7.13: Diffusivity values obtained from data measured by sensors of *"third array (A3)"*.

Considerations on results

The results obtained in this case are similar to the previous ones. It is possible to notice that the thermal diffusivity values obtained are in the same values range of the values obtained according to the first fibres placement. The variation of thermal diffusivity with distance is still evident.
The variability of the thermal diffusivity values obtained from all FBGs in different tests is less evident than the variability observed in the results of the previous tests. This could be a consequence of the better fixing of the fibres position using the acetate sheet.

7.2.3 The heating method - Second configuration tests

The figures 7.14, 7.15 and 7.16 show the thermal diffusivity values obtained from the data acquired from sensors closer to the source of each array (respectively A1, A2 and A3) in all the tests performed with second fibres configuration. The abscissa in figure 7.10 reports the x-distances of each sensor from the delivery fibre direction. The abscissa in figures 7.11 and 7.12 reports instead the y-distances of each sensor from the delivery fibre end (Fig. 7.8).

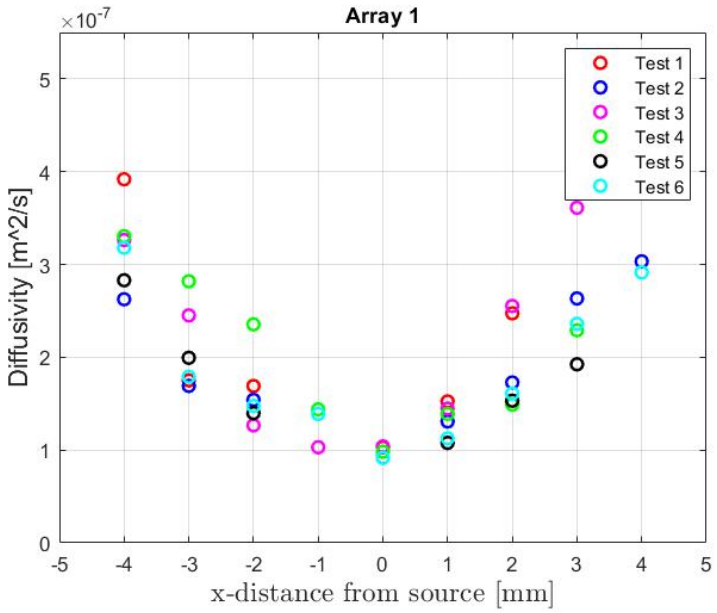

Figure 7.14: Diffusivity values obtained from data measured by sensors of *"first array (A1)"*.

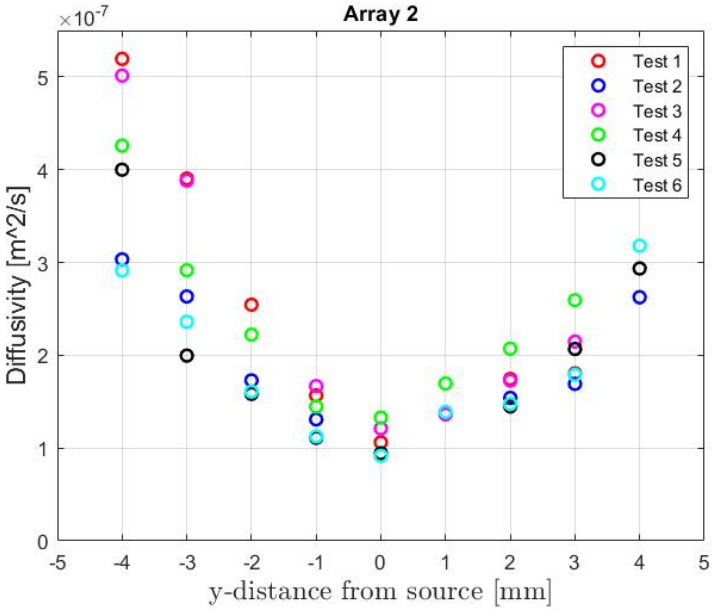

Figure 7.15: Diffusivity values obtained from data measured by sensors of *"second array (A2)"*.

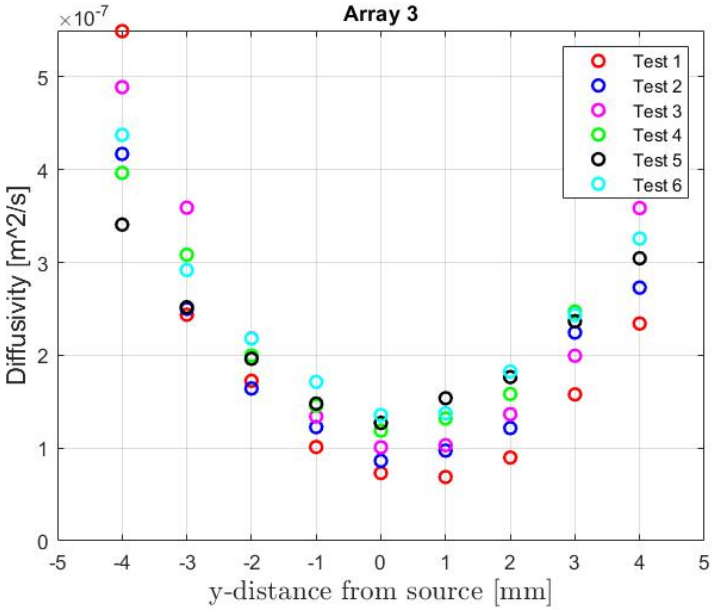

Figure 7.16: Diffusivity values obtained from data measured by sensors of *"third array (A3)"*.

Considerations on results

The parabolic trend is evident also processing the data using the heating method. The values of thermal diffusivity obtained are greater that the previous ones. this could be the result of an imperfect modeling of the source.

Chapter 8

Conclusions and future development

The biggest limitation of the liver tumors laser ablation consists in the lack of a treatment planning tool due to the difficulty to predict the outcomes given the large variability of the optical and thermal parameters of the liver tissue. This implies the necessity to find methods to evaluate these properties in order to optimize the ablation strategies.

This Master's thesis focused on finding and validating methods to evaluate thermal properties of ex-vivo bovine liver, mainly the thermal diffusivity. The Green's function method presented, proved to be valuable for this purpose. This method allows calculating the thermal diffusivity values processing the temperature variations experimentally recorded after inducing a small heating of the tissue by irradiating it with a laser source. Both heating and cooling curves have been used to calculate thermal diffusivity values using different data processing approaches.

Among the results presented in sections from 7.2.1 to 7.2.3 two main aspect are highlighted:

- the thermal diffusivity lies on a parabolic pattern over the distance;
- all the obtained values are within the range $0.02\,\mathrm{mm^2\,s^{-1}}$ to $0.5\,\mathrm{mm^2\,s^{-1}}$

The parabolic trend can be explained making some considerations on the distances between the sensors and the heat source and the tissue thickness involved in the tests.
As each slice of tissue is 4 mm thin and the sensors arrays used are 2 cm long, there is a certain amount of FBGs whose distances from the source are comparable or even greater than the thickness itself. When this occurs, the approximation of

infinite medium on which the method is based is not valid anymore, since energy losses at the boundaries become relevant.

Some more considerations can be made about the range of values obtained.
The range of thermal diffusivity values reduces to $0.02\,\mathrm{mm^2\,s^{-1}}$ to $0.25\,\mathrm{mm^2\,s^{-1}}$ considering only the results of the cooling approach. The expansion of the range due to the results of the heating approach may highlights the critical issues of the latter processing method, such as the possibility that the used source can not be modeling as a Gaussian distributed source in space and/or a rectangular source over the time. The range of thermal diffusivity values reduces even more considering just the values obtained from the data acquired from the central sensors, whose distances from the source make valid the approximation of infinite medium.
As expected, the variability of the diffusivity values obtained from each FBG in different tests results smaller using the acetate sheet to fix the fibres placements.

All the values obtained are encouraging considering the fact that the thermal parameters for the liver tissue that can be found in literature [19], results in a thermal diffusivity value approximately equal to $0.15\,\mathrm{mm^2\,s^{-1}}$, which is widely included in the range found.
The results are also encouraging considering the many factors that may affect the experimental measurements such as the use of different and differently preserved ex-vivo bovine tissues during the tests, the lack of a real-time temperature of the tissue monitoring during the heating phase or the absence of an automatic control of the actual irradiation time using the laser source. Moreover, many simplifying assumptions have been made.

Although the method is still to be refined, it has proved effective as a starting point for understanding the variability of the thermal diffusivity of liver tissue. Probably, more accurate results could be obtained by placing more arrays or denser sensors arrays on the tissue near the source. As an alternative, the method could provide better results working on tissue slices having a grater thickness.
Interesting and more precise results could also be obtained from the heating data processing method. Other hypotheses about the nature of the source in space and time can be made.

The results obtained in this thesis project can be considered a starting point for evaluating the thermal diffusivity of the liver tissue in more realistic conditions, trying to model and simulate the actual biological phenomena that occur in vivo. They can also be used to predict different ablation procedures using a multi-physics model developed in COMSOL Multiphysics®.

New strategies can be adopted to align the sensing fibres in order to use also the finite difference method developed, which would not require to model an impulsive source.

Bibliography

[1] URL: https://gco.iarc.fr/ (cit. on pp. 1–3).

[2] URL: https://www.airc.it/cancro/informazioni-tumori/guida-ai-tumori/tumore-del-fegato (cit. on pp. 1, 2, 4).

[3] Rebecca L Siegel, Kimberly D Miller, Hannah E Fuchs, and Ahmedin Jemal. «Cancer Statistics, 2021». In: *CA: a cancer journal for clinicians* (2021), pp. 7–33. ISSN: 0007-9235. DOI: 10.3322/caac.21654. URL: https://doi.org/10.3322/caac.21654 (cit. on p. 2).

[4] Muneeb Ahmed. «Image-guided tumor ablation: Standardization of terminology and reporting Criteria-A 10-year update». In: *Radiology* 273 (1 Oct. 2014), pp. 241–260. ISSN: 15271315. DOI: 10.1148/radiol.14132958 (cit. on pp. 5, 6).

[5] K. I. Ringe, M. Panzica, and C. Von Falck. «Thermoablation of Bone Tumors». In: *RoFo Fortschritte auf dem Gebiet der Rontgenstrahlen und der Bildgebenden Verfahren* 188 (6 June 2016), pp. 539–550. ISSN: 14389010. DOI: 10.1055/s-0042-100477 (cit. on pp. 6, 7).

[6] Sergio Sartori, Paola Tombesi, and Francesca Di Vece. «Radiofrequency, microwave, and laser ablation of liver tumors: time to move toward a tailored ablation technique?» In: *Hepatoma Research* 1 (2 2015), p. 52. ISSN: 2394-5079. DOI: 10.4103/2394-5079.155697 (cit. on pp. 6, 7).

[7] Riccardo Gassino, Yu Liu, Maria Konstantaki, Alberto Vallan, Stavros Pissadakis, and Guido Perrone. «A fiber optic probe for tumor laser ablation with integrated temperature measurement capability». In: *Journal of Lightwave Technology* 35 (16 Aug. 2017), pp. 3447–3454. ISSN: 07338724. DOI: 10.1109/JLT.2016.2618618 (cit. on p. 7).

[8] URL: https://www.physics-and-radio-electronics.com/physics/laser/laser-populationinversion.html (cit. on p. 13).

[9] Daniela Lo Presti et al. «Fiber Bragg Gratings for Medical Applications and Future Challenges: A Review». In: *IEEE Access* (2020), pp. 156863–156888. DOI: 10.1109/ACCESS.2020.3019138 (cit. on pp. 18, 21, 22).

[10] URL: http://www.infibratechnologies.com/technologies/fiber-bragg-gratings.html (cit. on p. 18).

[11] URL: https://www.aos-fiber.com/eng/Sensors/Sensoren.html (cit. on p. 19).

[12] Andreas Othonos. «Fiber Bragg gratings». In: *Review of scientific instruments* 68 (12 1997) (cit. on pp. 19–21).

[13] Jasjot K. Sahota, Neena Gupta, and Divya Dhawan. «Fiber Bragg grating sensors for monitoring of physical parameters: a comprehensive review». In: *Optical Engineering* 59 (06 June 2020), p. 1. ISSN: 0091-3286. DOI: 10.1117/1.oe.59.6.060901 (cit. on p. 21).

[14] Aurora Bellone. «Optical fibre sensors for distributed temperature monitoring during mini-invasive tumour treatments with laser ablation». Master's degree thesis. Politecnico di Torino, 2020 (cit. on p. 23).

[15] Ludovica De Sanctis. «Sensori di temperatura in fibra ottica quasi-distribuiti basati su reticoli di Bragg». Master's degree thesis. Politecnico di Torino, 2021 (cit. on p. 25).

[16] URL: http://www.ingaero.uniroma1.it/attachments/2176_Cap_1_Heat%5C%20Conduction%5C%20in%5C%203D%5C%20Solids.pdf (cit. on p. 26).

[17] URL: https://cecs.wright.edu/~sthomas/htchapter02.pdf (cit. on p. 28).

[18] URL: https://en.wikipedia.org/wiki/Green%5C%27s_function (cit. on p. 29).

[19] Alessandra Beccaria. «Studio teorico e sperimentale del comportamento termo-ottico di tessuti biologici per il trattamento di tumori mediante ablazione laser». Master's degree thesis. Politecnico di Torino, 2019 (cit. on p. 65).